A High-Resolution EUV Zinc-Oximate Resist: Why Post-Exposure Bake Fails to Improve Lithography Performance

Journal:	*The Journal of Physical Chemistry*
Manuscript ID	jp-2026-00751q
Manuscript Type:	Article
Date Submitted by the Author:	03-Feb-2026
Complete List of Authors:	Chen, Ying-Lin; Interuniversitair Micro-Elektronica Centrum, Advanced patterning Holzmeier, Fabian; imec, Fallica, Roberto; Interuniversitair Micro-Elektronica Centrum, Nathanael, Tan Manuel Marcello; IMEC Fernandes, Fernando; Universite catholique de Louvain, IMCN-NAPS Hackens, Benoit; Universite catholique de Louvain, Electrical Engineering Singh, Dhirendra; IMEC, MSP Conard, Thierry; IMEC Tseng, Li-Ting; PiBOND Gädda, Thomas; PiBOND Seefried, Sarah; PiBOND Han, Zhongmei; PiBOND De Gendt, Stefan; IMEC, Dorney, Kevin; imec vzw, Angstrom Patterning De Simone, Danilo; IMEC,

A High-Resolution EUV Zinc-Oximate Resist: Why Post-Exposure Bake Fails to Improve Lithography Performance

Ying-Lin Chen,[*,†,‡] Fabian Holzmeier,[‡] Roberto Fallica,[‡] Tan Manuel Marcello Nathanael,[‡,¶] Fernando M. Fernandes,[¶] Benoit Hackens,[¶] Dhirendra P. Singh,[‡] Thierry Conard,[‡] Li-Ting Tseng,[§] Thomas M. Gädda,[§] Sarah Seefried,[§] Zhongmei Han,[§] Stefan De Gendt,[†,‡] Kevin Dorney,[‡] and Danilo De Simone[*,‡]

†*Sustainable Chemistry for Metals and Molecules, KU Leuven, Belgium*

‡*imec, Kapeldreef 75, 3001 Leuven, Belgium*

¶*Nanoscopic Physics (NAPS), IMCN, UCLouvain, 2 Chemin du cyclotron, 1348 Ottignies-Louvain-la-Neuve, Belgium*

§*PiBond, PiBond Oy, Kutojantie 2 B, FI-02630 Espoo, Finland*

E-mail: ying-lin.chen@imec.be; Danilo.DeSimone@imec.be

Abstract

Zinc oximates — organometallic compounds combining zinc and oximate ligands— were previously used as precursors for zinc-oxide-based thin-film transistor applications. Recently, the potential of zinc oximates as high-resolution patterning materials was evaluated via electron beam and extreme ultraviolet (EUV) lithography (EUVL). However, a detailed understanding of the lithographic reaction mechanisms is currently lacking due to limited exploration in material characterization and process tuning, particularly the crucial reaction mechanism that occurs during the post-exposure bake (PEB).

Understanding how PEB affects zinc oximate resists is essential to further enhance EUV sensitivity and line edge roughness of this potentially new class of organometallic resists. In addition, the integration of zinc oximate resists into industrial EUV lithography processes has not yet been demonstrated. To address this knowledge gap, we first demonstrated the highest resolution possible (pitch-24-nm line-and-space) with a 0.33NA ASML EUV scanner tool, then performed a holistic investigation of the EUV exposure and thermally-driven reaction mechanisms of a zinc oximate resist, ZONE (Zinc Open-source Nano-Engineered), which we link to on-wafer pitch-32-nm dense line-and-space EUV patterning performance. Specifically, we show that thermal treatment at 140° C temperatures leads to the initiation of conversion into ZnO, thus preventing the optimization of patterning performance via the PEB. In contrast, no ZnO formation is observed under EUV exposure of 100 mJ/cm^2, indicating a fundamentally different mechanism for the solubility switch—one driven by preferential bond cleavage rather than bulk oxide formation. These competing chemical mechanisms manifest in a degradation of pattering performance (e.g., resolution, line-edge roughness, etc.) under increasing PEB temperature (from 120°C to 180° C), which indicates thermally-driven reactions indiscriminately cleave organic bonds and compromise the solubility contrast in ZONE. Nevertheless, the remarkably high resolution in EUV lithography suggests that metal oximate resists are a promising platform for future high-NA EUV lithography.

Introduction

As semiconductor manufacturers continue to shrink device dimensions in accordance with Moore's law,[1] the demand for novel photoresists[2] capable of achieving both higher resolution and sensitivity remains strong. Resolution determines the smallest printable feature, while sensitivity directly affects wafer throughput in lithography scanners.[3] In EUVL, the energy of EUV photons (∼92 eV at 13.5 nm) is significantly higher than in Deep Ultraviolet (DUV) (∼6 eV at 193 nm). As a result, the number of photons delivered at the same dose is about 14

times lower in EUV than in DUV, leading to stochastic failures caused by photon shot noise.[4] This photon shot noise increases the line-edge roughness (LER) of the patterned resist. To improve LER, lithographers often increase the exposure dose, leading to the well-known RLS (Resolution, LER, Sensitivity) trade-off.[5] Therefore, increasing the EUV photon absorption in the resist layer can lower the exposure dose without sacrificing resolution or sensitivity, a key objective in high volume manufacturing.

Chemically amplified resists[6] have been the workhorse of current EUV lithography processes. A typical CAR formulation includes a photoacid generator (PAG), copolymer matrix, and a base quencher. PAGs amplify the EUV photon signal by generating acid in response to secondary electrons produced during EUV exposure.[7] These acids catalyze deprotection reactions within the matrix polymer, leading to solubility changes. However, excessive acid diffusion can cause undesired solubility switches far from the exposure site. Quenchers are therefore incorporated to neutralize excess acid and mitigate these effects.[8] Since CARs are multicomponent mixtures, scaling down to the smaller resist volumes required for high-numerical-aperture (NA = 0.55) patterning introduces chemical stochastic effects.[9,10] This has motivated the interest to develop single-component EUV photoresists, which can potentially alleviate the chemical stochasticity as compared to CARs and reduce the size of the effective patterning unit (e.g., the molecular size).[11] In addition, the photon shot noise, described previously, propelled the exploration of incorporating metal atom into photoresists.

In recent years, organometallic resists[12] have gained increasing attention because of their high sensitivity, potential for high resolution and low roughness (from smaller molecular size), and low chemical stochastics (from its single component). Furthermore, the improved EUV absorption and etch resistance[13] of metal-containing resists make them well-suited for high-NA EUVL, where thinner resist films are more suited to shallower depth of focus.

To date, organometallic zinc oximates have mostly been explored as precursors for the generation of ZnO, rather than as EUV lithography materials. The mechanistic transformation from the zinc oximate to ZnO has mostly been studied by three known methodologies:

1) Chemical-vapor deposition (CVD)-based processes, 2) Thermal decomposition from spin-coated films, and 3) DUV decomposition at very high dose. These materials were first introduced as single-source CVD precursors for ZnO deposition by Hill et al. in 2005.[14] Subsequent developments focused on tuning alkyl ligands to improve ZnO yield,[15] with 2-(methoxyimino)propanato zinc[16]—used in this study—offering the highest efficiency. This compound has also enabled DUV-patterned ZnO-based thin-film transistors such as zinc tin oxide and indium zinc oxide.[17] Interestingly, thermal decomposition at 150°C favors a (002) crystal orientation, while DUV-induced decomposition produces more amorphous films with improved surface roughness.[18] The ability of zinc oximates to transition from organic containing single molecules to a highly inorganic ZnO structure (e.g., a solubility change) provides an intriguing pathway for their use as lithographic materials. Recently, 2-(methoxyimino)propanato zinc and related oximate compounds have shown promising high-resolution performance as negative-tone resists in electron beam lithography (EBL) and EUV interference lithography (EUV-IL).[19] However, comprehensive material characterization and systematic process evaluation—particularly the role of post-exposure bake (PEB), a critical step in resist processing[20]—have not been addressed so far.

Baking steps are important in photolithography. The post-application bake (PAB), applied after spin-coating of the photoresist film, is primarily used to remove residual solvent and improve the film adhesion on the substrate.[21] The PEB, conducted after light exposure, accelerates the chemical amplification in conventional CARs by promoting acid-catalyzed deprotection reactions and acid diffusion.[5] Previous studies on tin-oxo cage resists have shown that an optimized PEB can improve the pattern contrast and reduce the required exposure dose.[22] In the study by Needham et al.,[23] both experimental and modeling results demonstrated that thermal baking after EUV exposure enhances the lithographic sensitivity of metal oxide resists by promoting ligand cleavage and generating active sites for the condensation-driven formation of a metal-oxo network. Therefore, it is important to examine whether zinc oximates exhibit a similar mechanism, where thermal baking enhances the

chemical contrast generated during EUV exposure.

In this paper, we adopted a zinc oximate with both R_1 and R_2 groups to be methyl groups, also known as 2-(methoxyimino)propanoato zinc as shown in Fig. 1, to which we will refer to as ZONE (Zinc Open-source Nano-Engineered). We first demonstrate that the ZONE resist achieved the highest resolution available in a 0.33 NA EUV lithography scanner, pitch-24-nm lines and spaces (L/S), showing its potential for high-NA applications. Yet, a very high EUV dose ($>140 mJ/cm^2$) was necessary to successfully pattern ZONE at this resolution. To study the potential to enhance the sensitivity, the effect of the PEB was investigated for pitch-32-nm L/S patterning; however, the sensitivity and roughness were not improved for the ZONE resist. To further understand this lack of lithographic performance improvement (as typically observed for other resist classes), the thermal decomposition was analyzed for ZONE during thermal processes of lithographic relevance, e.g., lasting 1 minute. X-ray Photoelectron Spectroscopy (XPS), Fourier Transform Infrared Spectroscopy (FTIR), Spectroscopic Ellipsometry (SE), EUV-induced outgassing mass spectroscopy, and surface energy analysis were employed for the material characterization. These same techniques were then also used to characterize the resist after solely EUV exposure, allowing us to directly compare thermal and photochemical pathways. Through this coordinated analysis, we revealed that there are intrinsic differences between thermal decomposition and EUV-induced reaction. Therefore, the PEB, the traditional sensitivity enhancing process step for CARs and metal oxide resists, should be carefully considered in the present material and the possible variations of it.

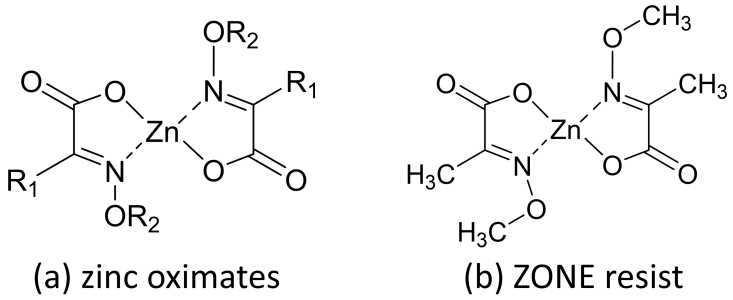

Figure 1: Chemical structures of (a) a generic zinc oximate with various R1 and R2 substituents, and (b) the ZONE resist with both $R_1 = R_2 =$ methyl.

Methodologies

Sample preparation

In our experiments, two resist thicknesses were employed. For film characterization techniques such as FTIR, XPS, and ellipsometry, a 38 nm film was used to increase the signal strength. For lithographic evaluation, a thinner resist layer of 29 nm was chosen to optimize patterning performance. In EUVL, typical resist thicknesses for (L/S) patterning range from 22 to 35 nm.[24,25] To study the effect of PAB, a bake duration of 1 minute was selected, which falls within the typical range used in lithographic processes (few tens of seconds to several minutes). Sample sizes were adjusted according to the requirements of the individual tools to ensure compatibility across all measurements. An overview of the sample preparation conditions is described in Table 1.

P24 L/S EUV patterning wafer: A 29 nm film of ZONE resist was spin coated at 1500 rpm for 60 seconds directly on 300 mm Si wafer. PAB was 50°C for 1 minute. Before spincoating, a dehydration bake of 205 °C was applied to the wafer. The wafer was exposed in a NXE3400:B EUV scanner with a specialized illumination pupil for high resolution P24 L/S patterning.[26] No PEB was applied, and the wafer was developed using DP819A from Fujifilm[27] for 15 seconds without rinse. A longer development time compared to 10 seconds

Table 1: A summary of sample preparation. For L/S EUV patterning, we used a focus-exposure matrix (FEM)

Sample type	Substrate	Thickness	EUV tool	EUV exposure condition	PEB
P24 L/S EUV patterning	300 mm Si wafer	29 nm	NXE:3400B	L/S, FEM (100 to 180 mJ/cm^2)	No
P32 L/S EUV patterning	300 mm Si wafer	29 nm	NXE:3400B	L/S, FEM (60 to 150 mJ/cm^2)	No 120°C 140°C
Thermal degradation characterization (FTIR, XPS, Ellipsometry)	Coupons (3 cm × 3 cm)	38 nm	No	N/A	From 70 to 220°C
Thermal degradation (Surface energy)	100 mm Si wafer	38 nm	No	N/A	180°C
Characterization (FTIR, XPS, Ellipsometry)	300 mm wafer & coupons (3 cm × 3 cm)	38 nm	NXE:3400B BEFORCE	Open-frame at 0 to 150 mJ/cm^2	No
EUV-induced outgassing	200 Si wafer	38 nm	BEFORCE	EUV beam scanning	No
Thermal outgassing	Coupons (2 cm × 2 cm)	38 nm	No	N/A	Increasing slowly

for P32 L/S was used to improve the pattern quality by reducing the shot noise: with longer development, a higher exposure dose is required to achieve the same critical dimension, which in turn lowers shot noise. The resulting resist pattern was examined using a Critical Dimension Scanning Electron Microscope (CD-SEM).

P32 L/S EUV patterning wafers at different PEB conditions: Three wafers were prepared under the same conditions as described in the previous section. The wafers were again exposed under the same conditions using the same illumination pupil optimized for L/S patterning. Then, all three wafers were developed by DP819A for 10 seconds. All three wafers were reviewed by CD-SEM using the same recipe.[28]

Characterization of the thermal degradation mechanism in ZONE: Samples were prepared for each different characterization technique slightly differently as mentioned below:

1. FTIR, ellipsometry, and XPS analysis: A 38 nm film of ZONE resist was spincoated directly on a 300 mm Si wafer. The PAB was 50 °C for 1 minute. The wafer was cleaved into 3 cm X 3 cm coupons. Each coupon was then baked at a different temperature, from 70 to 220 °C using 5 °C intervals (between 70-180 °C) and 10 °C intervals (between 180 to 220 °C). FTIR was measured immediately after baking. Ellipsometry

was measured at the center of the coupons, the beam spot size was around 3 to 4 mm (depending on angle of incidence). Only the samples baked at a temperature of 120, 140, and 180 °C were selected for XPS analysis. Those samples were further cleaved into 1 cm X 1 cm sized coupons.

2. Surface energy analysis: A 38 nm film of ZONE was spincoated on two 100 mm Si wafers and a PAB at 50 °C for 1 minute was applied. One wafer directly underwent a contact angle measurement for surface energy analysis and the other one was baked at 180 °C for 1 minute before the contact angle measurement.

3. Thermal outgassing: A 38-nm ZONE film was spincoated on a 200 mm wafer and cleaved into 2 cm X 2 cm coupons for thermal outgassing in home-built high-vacuum temperature-programmed desorption instrument.

Characterization after EUV exposure: Samples (coupons and wafer) were prepared differently as mentioned below:

1. FTIR with BEFORCE tool:[29] A 38 nm film of ZONE resist was coated on 3 cm X 3 cm coupons and a PAB at 50 °C was applied for 1 minute.

2. EUV-induced outgassing: A 38 nm film of ZONE resist was coated on a 200 mm wafer and a PAB at 50 °C was applied for 60 seconds.

3. FTIR and ellipsometry with NXE open-frame exposure: A 38 nm film of ZONE resist was coated on 300 mm wafer and a PAB at 50 °C was applied for 1 minute. Thickness uniformity was confirmed on 49 points spectroscopic ellipsometer (wavelength: 240 to 900 nm). The wafer was sent to open-frame exposure in NXE scanner, no baking and development were applied afterward. The wafer was cleaved into 3 x 3 cm coupons for the succeeding measurements. To extract the optical band-gap, a RC2 ellipsometer from J. A. Woollam was used to determine the optical constants, n and k.

Analysis methods

To gain a comprehensive understanding of the patterning behavior under different PEB conditions and to investigate the underlying chemical mechanisms during baking and EUV exposure, various analytical techniques were employed. FTIR was used to monitor changes in vibrational bonding states during both thermal and EUV treatments. XPS provided insights into the atomic composition and chemical bonding within the resist film. Additionally, EUV- and thermally-induced outgassing spectra were analyzed to identify volatile species released during baking and EUV exposure. The film thickness and the complex refractive index were evaluated using spectroscopic ellipsometry. For lithographic assessment, an ASML NXE scanner was used for EUV exposure, and CD-SEM was employed to evaluate the patterning performance of the ZONE resist.

FTIR: Wafer-level FTIR measurements were initially conducted to quickly assess the chemical changes induced by EUV exposure using the NXE scanner. To achieve higher spectral resolution and improved signal quality, especially for both thermal and EUV-induced effects, FTIR measurements were also performed on small coupons under vacuum conditions. The reduced ambient interference in vacuum enabled more precise detection of vibrational changes. In contrast, the wafer-level measurements were performed in a cleanroom environment under ambient pressure.

1. Wafer-level measurement: A commercial FTIR spectrometer (Nicolet iS50, Thermo Fisher Scientific) with a motorized wafer table was used to conduct measurements at the given exposure sites. The wafer is held in a clean room atmosphere, and to alleviate the atmospheric absorption, a nitrogen purge flow of 40 standard cubic feet per hour was used. The spectra were collected by integrating 64 scans with a resolution of 4 cm^{-1} and the atmospheric suppression activated. Background subtraction was done by measuring the unexposed region after development, where ellipsometry showed that the resist was completely removed.

2. Coupon measurement: A commercial FTIR spectrometer (iG50, Thermo Fisher Scientific) was used for FTIR measurements. The samples were placed in a custom-built sample chamber at a pressure of <0.1 mbar to avoid absorption of atmospheric species. Additionally, an N_2 purge is applied between the source and detector optics of the FTIR. To increase the signal, the samples are inclined at an angle of 30°with respect to the incident IR beam. The spectra were collected by integrating 128 scans with a resolution of 4 cm^{-1}. A bare double-side polished silicon coupon was used for background subtraction.

X-ray photoelectron spectroscopy (XPS): The measurements were carried out in angle-integrated mode using a QUANTES instrument from Physical electronics. 1 cm X 1 cm samples were used for the measurement employing an Al Kα radiation source of 1486.6 eV with a spot size of 100 µm. The spectra of C 1s, N 1s, O 1s, and Zn $2p_{3/2}$ were recorded. Charge neutralization during measurement was achieved using an electron flood gun, minimizing peak shifts associated with the insulating properties of the ZONE resist. The photon energy of the raw spectra was calibrated on the C1s peak at 284.8 eV in the CasaXPS software.

EUV-Induced Outgassing mass spectra: EUV induced outgassing was measured in the BEFORCE tool at imec,[29] where an integrated Pfeiffer QMG422 quadrupole mass recorded the outgassed mass species. The mass spectra were measured while an EUV beam scanned a 200 mm wafer coated with ZONE resist. The scanning rate was chosen such that the resist experiences an EUV dose of 7 mJ/cm^2. 11 cycles between 0 to 120 amu were used to average the outgassing signal. A detailed description of the method can be found in ref.[30]

Thermal-Induced Outgassing mass spectra: The temperature programmed desorption experiments were conducted at Winfab (Wallonia Infrastructure for Nano FABrication), UC Louvain, using a homebuilt setup to monitor resist outgassing upon heating. In brief, a

resist-coated silicon coupon was mounted upside down in a vacuum chamber reaching a base pressure of approximately $8.7 \cdot 10^{-6}$ mbar. The coupon was then heated by a 15 V, 150 W Osram halogen lamp positioned outside of the chamber in front of a Pyrex window and the temperature of the sample was measured by a type-K thermocouple attached to its backside. Both the power supply of the halogen lamp as well as the thermocouple were connected to a proportional-integral-derivative (PID) controller (Eurotherm 818R) to hold the temperature stable. The probe of the residual gas analyzer (Stanford Research Systems RGA100) was placed in between the front side of the coupon and the turbomolecular pump and the ion signal was recorded as a function of the thermocouple temperature.

BEFORCE EUV exposure: EUV exposures were done on the IMEC BEFORCE tool, where, after exposure, the sample was transported under vacuum into the FTIR chamber, therefore minimizing the interference of the environment. The integrated Energetiq's EUV source (EQ-10) was used for the exposure. The EUV exposure dose is controlled via continual monitoring of the EUV flux and exposure times are adjusted based on the monitored EUV flux to achieve the desired dose. More details can be found in Pollentier et al. (2025).[29]

Spectroscopic ellipsometry: A RC2 ellipsometer from J. A. Woollam[31] was used to measure the thickness and the refractive index of the samples. The measurements were done at the center of 3 cm X 3 cm silicon coupons at 60 °, 65 °, and 70 ° angle of incidence per point. The beam size was about 3 to 4 mm in diameter. A Cauchy model was used to determine the film thickness from spectra of 400 nm to 1000 nm at three different angles. Only the parameters A and B of the Cauchy model, and the thickness were chosen as free fitting parameters. To determine the band-gap of the material, the thickness was fixed after the Cauchy fitting and a B-spline model was built with a resolution of 0.05 eV. To ensure the b-spline model remained physically realistic, the imaginary part of the dielectric constant was constrained to be positive. Since the exact bandgap position was unknown, we assumed transparency only in the 400 nm to 1000 nm range and allowed the model to determine the

refractive index for the absorptive region (< 400 nm).

Surface energy analysis: OCA020 from Dataphysics[32] was used to determine the contact angle of water and diiodomethane on the substrate. Five droplets with a volume of 1 µL were used for each liquid. The built-in software SCA20 was used to determine the contact angle of water and diiodomethane. The OWRK model substituted into Young's equation yields a linear equation for solving dispersive and polar components of the surface.[33] The surface energy of the reference liquids was taken from Kaeble (1970).[34]

EUV exposure in NXE3400B: An ASML NXE:3400B[35] EUV scanner featuring an NA=0.33 was used for two purposes:

1. EUV lithography for line-and-space patterning, where a dark-field mask was used for the patterning. A Focus-Exposure Matrix was used to find the best dose and focus for the patterning. The NXE3400:B scanner was connected to a commercial LITHIUS track from TEL, ensuring minimal delay between EUV exposure and development.

2. FTIR ligand signal calculation after EUV exposure, where an open-frame mask was used to expose with doses between 20 mJ/cm^2 to 200 mJ/cm^2. The exposed regions were later cleaved into coupons. Each exposure die size was 12 mm X 12 mm.

CD-SEM: A CG6300[36] CD-SEM from Hitachi was used for inspecting line-and-space patterns. The image field of view was 0.819 µm x 0.819 µm with a pixel resolution of 1024 X 1024 and magnification of 164.8K. Voltage and current were chosen as 500V and 8.0 pA, respectively. 16 frames were acquired for each image and analyzed using the software Fractilia[37] for CD and uLER (unbiased line-edge roughness) extraction.[28]

Results & Discussion

P24 L/S patterning: Highest resolution in 0.33NA scanner

To prove the high resolution potential of the ZONE resist for wafer-level processing, we challenged the ZONE resist to resolve the highest L/S resolution available in the NXE:3400B scanner, pitch-24-nm (P24) L/S. Employing the conditions described above, a P24 L/S pattern with low uLER of 1.97 ± 0.12 nm was printed, as shown in Fig. 2. This result shows that the reaction triggered by the aerial images is projected very locally onto the resist, therefore providing a high-resolution pattern. From these results and the one shown by Saifullah et al. (2024)[19] using EUV interference lithography (EUV-IL), it becomes evident that the ZONE resist, and possibly zinc oximates materials in general, contain great potential for high resolution patterning in high-NA EUVL. However, this required a high exposure dose of 148 mJ/cm^2, which is disadvantageous for high-volume-manufacturing. To address this sensitivity issue, different PEB conditions, which potentially facilitate the pattern formation with moderate thermal ligand cleavages, were evaluated.

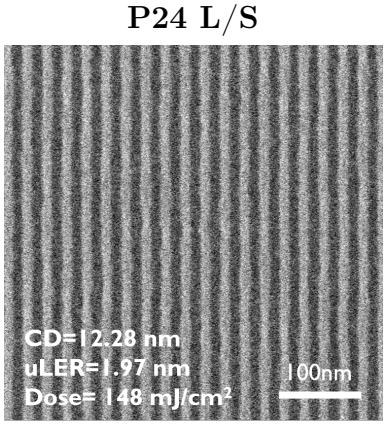

Figure 2: CD-SEM image of P24 L/S pattern. The development time was 15 seconds.

P32 L/S EUV patterning at different baking conditions

To understand the PEB effect, three PEB conditions were compared: no PEB, PEB at 120 °C for 60 seconds, and PEB at 140 °C for 60 seconds. 120 °C and 140 °C were selected because

we expected the thermal process to provide moderate ligand cleavage according to our prior knowledge from FTIR (see below). The targeted pitch for this comparison was chosen as pitch-32 nm L/S. A more relaxed pitch can yield more insights since the wider process window allows clearer observation of how parameter variations affect the patterning outcome. In contrast, using a challenging pitch can result in complete pattern failure even from minor parameter changes, offering little-to-no insight into the underlying process behavior.

As Fig. 3 (a) shows, without PEB, P32 L/S with CD=16.79 nm and uLER=2.11 ± 0.06 nm requires a dose of 106 mJ/cm^2. The LER was still measured to be low at this relaxed pitch, 2.11 nm, and the dose was reduced due to the shorter development time. If a PEB was applied, however, the L/S pattern degraded for increasing temperature. In Fig. 3 (b), showing the CDSEM image for a bake at 120 ° C, the uLER surged to 3.9 nm while the dose decreased to 94 mJ/cm^2, i.e., a dose reduction of only about 10 %. When the PEB temperature increased further to 140 °C, all the nano-scale L/S patterns failed as shown in Fig. 3 (c). Even at relax pitch-64-nm, no line-and-space was found. It is noticed that µm-scaled patterns, for example, the alignment mark were printed as shown in Fig. S1, indicating that the resist still showed a solubility switch, however degraded severely. Unlike tin-oxo cage resists,[22] little improvement can thus be achieved by PEB.

To better understand the failures of PEB in the ZONE resist system, several material characterization techniques were employed to understand how the ZONE resist reacts during thermal treatment and EUV exposure.

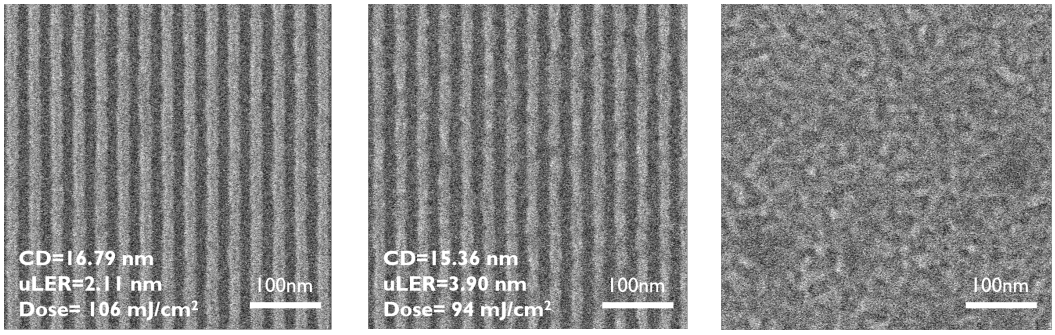

Figure 3: CD-SEM images of P32 L/S patterning with (a) no PEB, (b) PEB 120°C, and (c) 140 °C for 60 seconds.

Characterization of the thermal degradation mechanism in ZONE

Having demonstrated the high-resolution capability of the ZONE resist and the unexpected effect of PEB, we next aimed to understand why PEB fails to enhance the sensitivity. In this section, short thermal bakes (1 minute) at various temperatures were applied and the thermally-induced chemical and structural changes were probed. In the following section, similar methods will be used on samples subjected only to EUV exposure. Together, these studies provide a comprehensive view of the distinct mechanisms triggered by thermal and EUV photons.

FTIR spectra of ZONE after a 1 min bake at different temperatures without any further processing are shown in Fig. 4 (a). The black curve marks the FTIR signal for the film as coated, only a mild PAB at 50 °C was applied for solvent removal. An assignment of the peaks is shown in the figure. The ligand signal was analyzed by calculating the absorbance area under the respective peaks when baked between 70 °C to 220 °C. All the ligands followed almost identical depletion kinetics caused by thermal decomposition. About 10% of the ligands are lost at 120 °C and about 50% of the ligands are lost at 140 °C. All signals disappear after a bake at 180 °C. The result is shown in Fig. 4 (b), all ligand signal intensities were normalized to the one without additional baking.

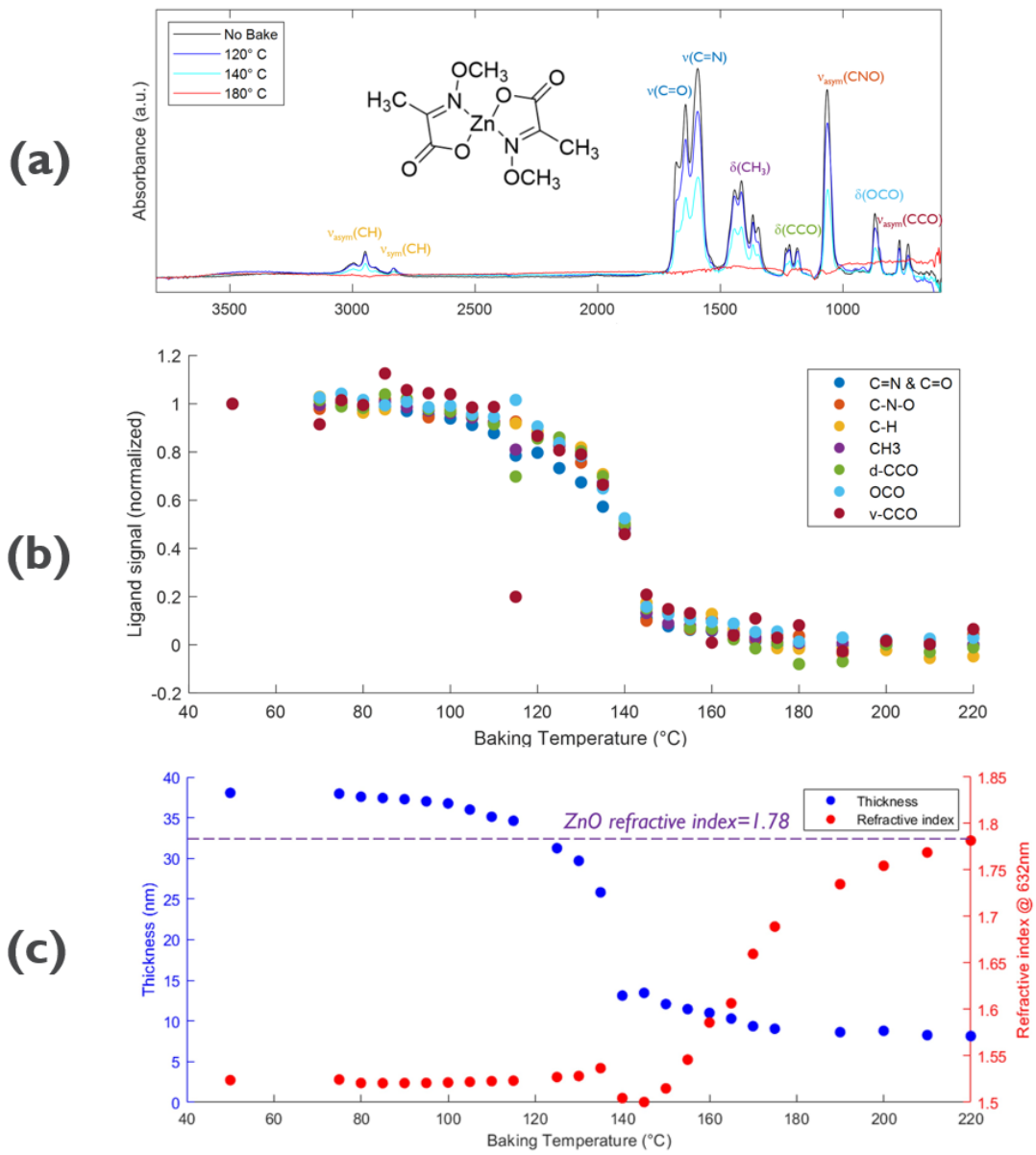

Figure 4: (a) FTIR spectra of unexposed ZONE with different baking temperatures: (black) No bake, (blue) 120°C, (light blue) 140°C, and (red) 180°C. The absorption peak assignments are labeled. (b) Evolution of the ligand signals as a function of baking temperature normalized to the unbaked sample. (c) Thickness and refractive index (@632 nm) as a function of baking temperature.

In Fig. 4 (c), the corresponding film thickness and refractive index (at 632 nm) was also determined by spectroscopic ellipsometry. The thickness loss sets in at 100 °C and at 140 °C more than half of the thickness is lost, which corresponds to the significant ligand loss

in Fig. 4 (b). The observed ligand signal profile and thickness profile after bake at different temperature agree well with the thermogravimetry (TG) curves in Schneider et al. (2009).[15]

The extracted refractive index when baked at 180 °C is 1.7, and 1.78 at 220 °C, which agrees very well with the refractive index for ZnO.[38] This infers that the material decomposes into zinc oxide after baking at 180 °C. We noticed that after baking at 200°C, the absorption coefficient, k, increased significantly for photon energies greater than 3.3 eV. This could relate to the formation of a bandgap in the material. To further estimate the bandgap, this data was used to generate a Tauc plot as shown in Fig.5, from which the band gap is determined to be 3.330 eV ± 0.001 eV, which agrees well with the band-gap of zinc oxide observed by Yeh et al. (2016).[39] However, for the ZONE resist as coated (blue dots), only an insignificant oscillation around 3.3 to 3.5 eV was observed. Therefore, the appearance of a bandgap at 3.3 eV is attributed to the formation of zinc oxide during the 1 minute bake at 200 °C.

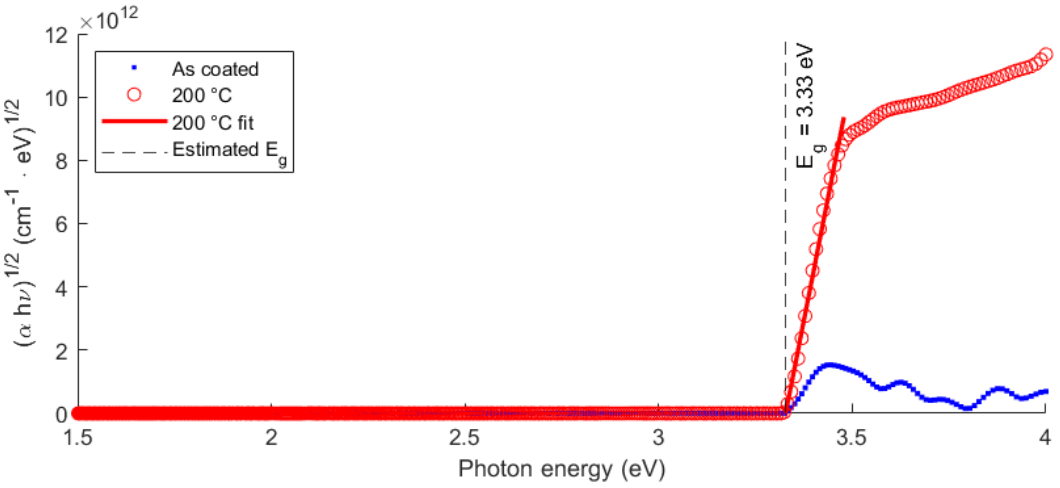

Figure 5: Tauc plot , i.e., the square root of the absorption coefficient multiplied by the photon energy $(\alpha h\nu)^{1/2}$ as a function of photon energy $(h\nu)$, for the as-coated ZONE film (blue points) and a sample baked at 200 °C (red points). A linear fit to the absorption edge of the baked sample (red line) allows the estimation of the optical band gap energy, E_g, by extrapolating to $(\alpha h\nu)^{1/2} = 0$, yielding $E_g \approx 3.330\,\text{eV} \pm 0.001\text{eV}$.

In the thermal outgassing measurement shown in Fig. 6, main fragments were detected at m/z = 29 (CH_2O), m/z = 32 (CH_3OH), m/z = 41 (CH_3CN), and m/z = 44 (CO_2), as expected.[16] All fragments follow a similar trend as a function of temperature and the highest

outgassing rate is measured for all fragments at around 150 °C, which corresponds to the sharpest decline of the ligand signals observed in FTIR (see Fig. 4 (b)). This observation matches the one from FTIR results. The majority of the organic ligands are thus lost at 140 to 150 °C at the same rate and there is no preference for the generation of a specific fragment. This explains the finding in Hoffmann and Schneider (2011)[18] that zinc oxide is formed during a low temperature bake at 150 °C for 10 minutes.

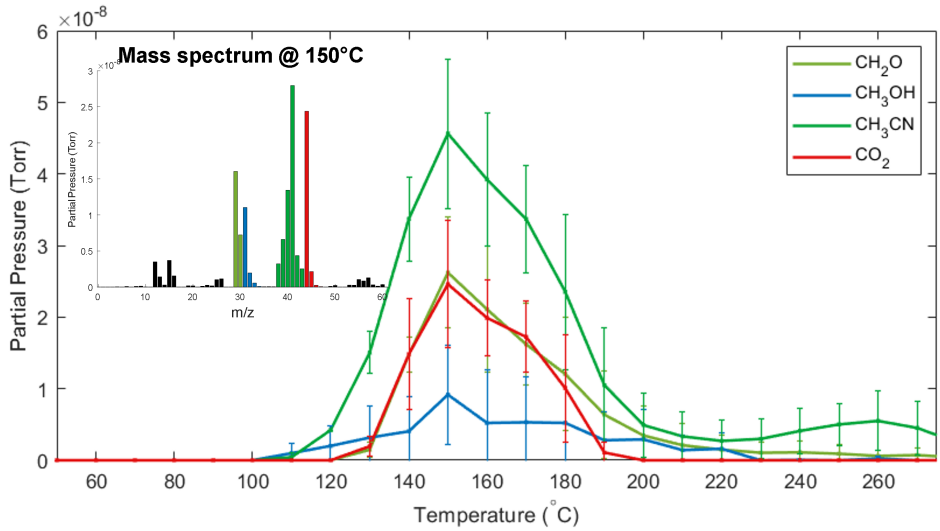

Figure 6: Intensity of outgassing fragments of the ZONE resist as a function of temperature. In the inset, the complete mass spectrum at 150°C is shown with the m/z assigned to the fragments highlighted in color.

In addition, XPS was measured for samples baked at different temperatures (as coated, 120°C, 140°C, and 180°C) for 1 minute. As shown in Fig. 7(a), the atomic ratios show a negligible variation for carbon and nitrogen after baking at 120 °C. Significant decreases in both carbon and nitrogen signals are observed when the bake temperature increases from 140 °C to 180 °C (80% of carbon and 90% of nitrogen), whereas the oxygen signal shows a relatively lower decrease. A deconvoluted view on the C 1s spectra is shown in Fig. 7(b). It indicates that all carbon peaks decay in a similar way as the baking temperature increases. The detailed analysis of the O 1s spectra is shown in Fig. 7(c) and three primary components were found: Peak 1 at 531.6 eV is attributed to oxygen bound to organic rests and metal

hydroxide species (e.g., O–N and C-O), peak 2 at 532.9 eV corresponds to carboxylate-like oxygen, and peak 3 at 530.0 eV is assigned to metal oxide (Zn–O). Baking at 120 °C results in no significant change in peak positions or relative intensities. However, at 140 °C, both the hydroxide/organic oxygen and carboxylate components decrease in intensity, accompanied by a corresponding increase in the metal oxide peak. This trend continues at 180 °C. These results indicate a gradual thermal transformation from the ZONE molecular structure to zinc oxide, beginning at temperatures of 140 °C. The concomitant loss of carbon- and nitrogen-containing species and the rise of Zn–O signal support a decomposition mechanism involving oxime ligand loss and metal-oxide formation. Finally, the surface energy of ZONE was checked before and after a bake of 180 °C. Before baking, the dispersive component was 23.03 mJ/m^2 and the polar component was 40.02 mJ/m^2. After baking, the dispersive and polar components were 31.94 mJ/m^2 and 12.37 mJ/m^2, which is very close to sputtered ZnO with 10% of O_2 reported in Najih et al.[40] This further supports the conclusion that ZONE was converted to ZnO upon brief thermal treatment.

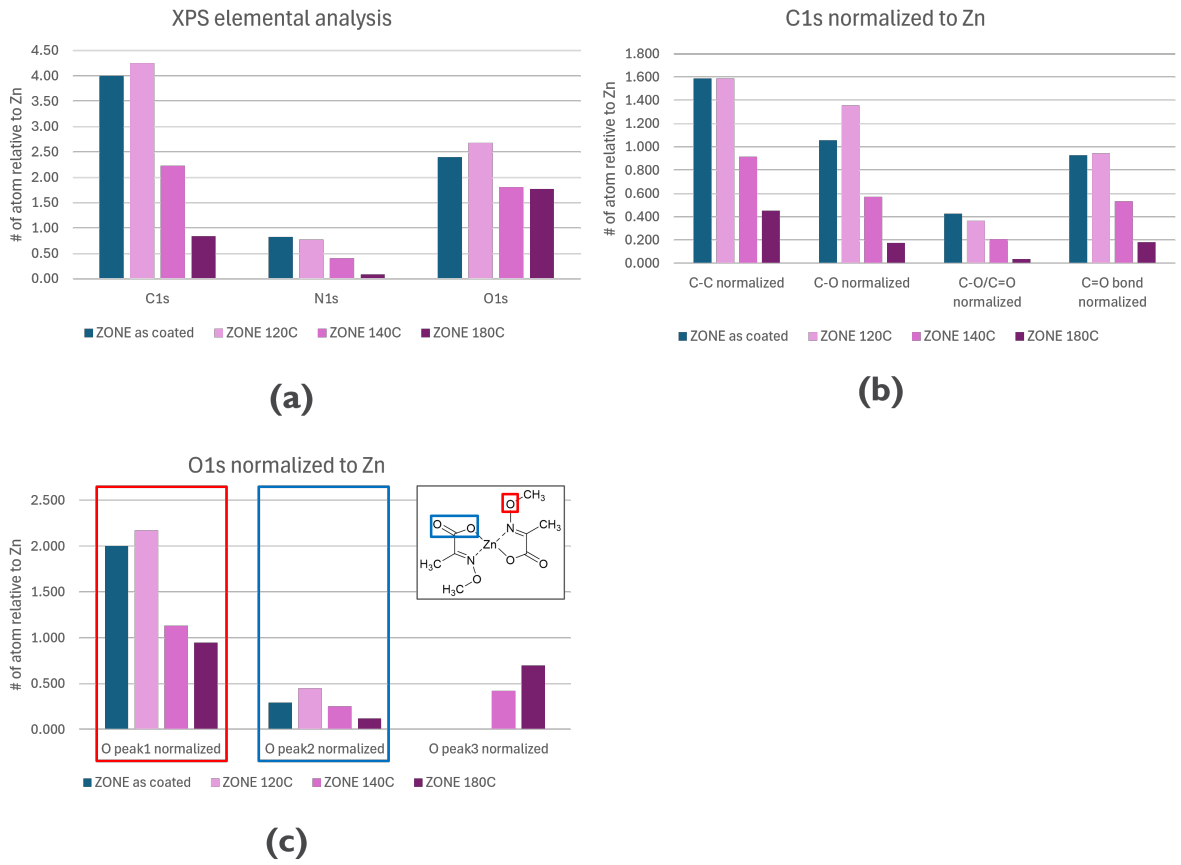

Figure 7: (a) XPS elemental analysis for a bake at different temperatures for 1 minute relative to Zn. When baked at 140 °C, a significant loss of carbon is observed. About 80% of carbon and 90% of nitrogen were lost after baking at 180 °C. (b) Deconvoluted C1s signal. (c) Deconvoluted O1s signal. (Detail fitting of the O1s signal in Fig. S9)

In summary, we found that the ZONE resist is not thermally stable even when baked only for a short time of 1 minute. Most of the film decomposes into zinc oxide at 180 °C to 200 °C as proven independently by the change of the refractive index, the occurrence of a band-gap matching zinc oxide, XPS, and the surface energy. It is thus confirmed that a thermal decomposition reaction takes place between 140 to 150 °C, as a significant ligand loss, thickness loss, and thermal outgassing is observed. Yet, a short baking of 1 minute at this temperature is not enough to convert the film completely into zinc oxide. However, substantial organic bond cleavage for all ligands is observed. Therefore, it can be stated that the baking temperature in the lithography process should never exceed 140 °C. Otherwise

the unexposed region might undergo a too vigorous undesired reaction.

Characterization of EUV-exposed ZONE

To understand how the ZONE resist reacts upon EUV irradiation, we measured the FTIR spectra immediately after EUV exposure in an EUV flood exposure tool. The doses were: 0 20, 40, 60, 100, and 150 mJ/cm^2. Fig. 8 shows FTIR spectra at different exposure doses. The film has a high organic content even after exposure at the highest dose, 150 mJ/cm^2. From a contrast curve obtained with the same tool it becomes obvious that at doses above 40 mJ/cm^2 it is completely condensed and there is no thickness loss when developed employing the commercial developer DP819A by Fujifilm[27] for 15 seconds (see Fig.S6). Already at the lowest dose, 20 mJ/cm^2, a clear signature of a N-H stretching band appears around 3200 cm^{-1}. Since the samples were transferred to the FTIR chamber directly under vacuum, the interference from clean room environment can be excluded and the N-H stretching band must therefore originate from a chemical transformation induced by the EUV light. When analyzing the kinetics of the different bands as a function of the dose by fitting the integrated ligand signals using an exponential formula, $e^{-C\cdot\mathrm{Dose}}$,[23] it becomes obvious that not all bands follow the same kinetics. For the fit, the ligand signals were normalized to those in the unexposed film. The parameter C is a constant reflecting how fast the ligands were cleaved upon EUV exposure. Detailed fitting results can be found in the supporting information Fig. S4.

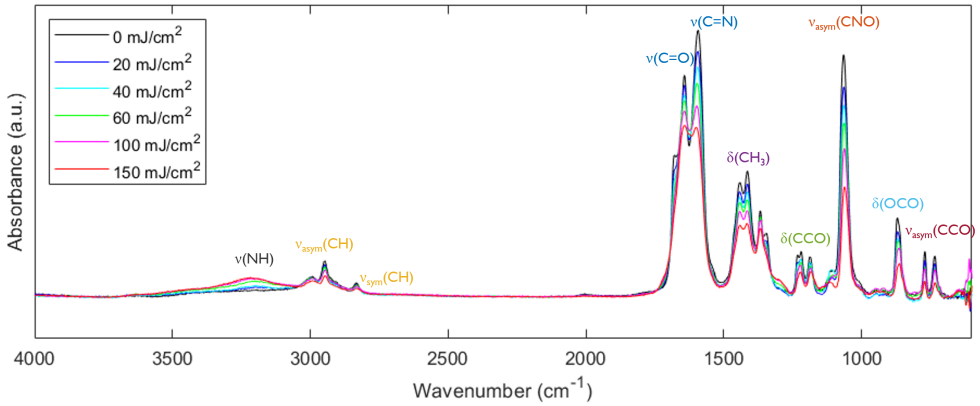

Figure 8: Evolution of the FTIR spectra of ZONE as a function of EUV dose. The main peaks are assigned to vibrational modes.

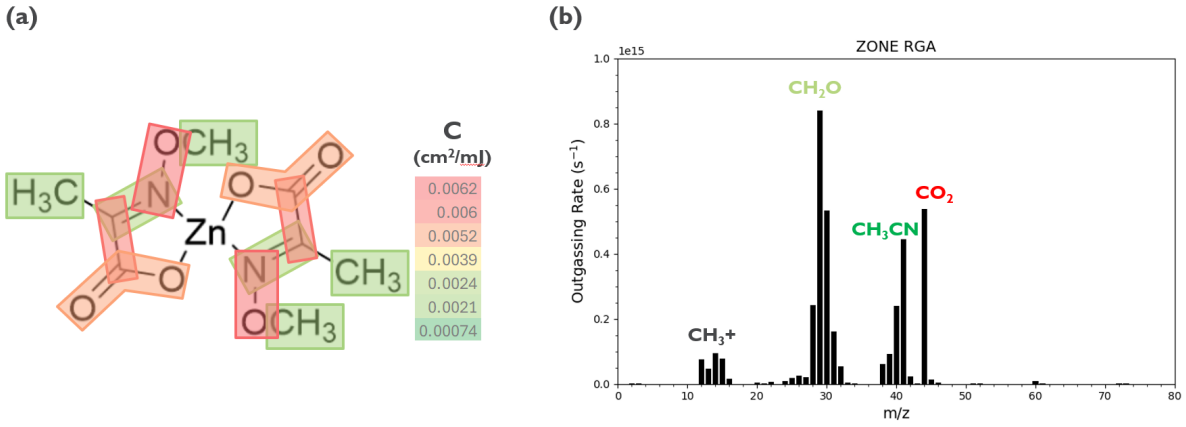

Figure 9: (a) Visualization of the kinetics observed in the IR spectra assigned to different parts of the molecule. The colormap represents the exponential constant C of the fit in cm^2/mJ of the FTIR peak area as a function of dose. The greater the C value, the faster the bond is cleaved during EUV exposure. (Detailed C values, see Fig. S4) (b) Outgassing mass spectra for ZONE under EUV exposure. The identified species match with the interpretation of the FTIR data. For more details about the assignment, see Fig. S7

The decrease of characteristic bands for all chemical bonds of the ligand, matches the observation in EUV-induced outgassing (see Fig. 9 (b)), where fragments corresponding to all parts of the ligand are observed with prominent peaks for carbon dioxide (CO_2, m/z=44), acetonitrile (CH_3CN, m/z=41,40,39,38), and formaldehyde (CH_2O, m/z=30,29,28). The formation of formaldehyde is not intuitive from the molecular structure of ZONE, but it was unambiguously identified by lowering the electron energy of the ionizer in the RGA (see Fig.

S8). It is assumed that formaldehyde originates from oxidation of the primary fragment methanol, possibly catalyzed on the surface of the resist film, similar to what has been observed on zinc oxide surfaces.[41] The loss of CH_2O could also be involved in a hydrogen transfer to the nitrogen, therefore forming the N-H bond observed in the IR spectrum.

We further looked at the optical properties analyzed from spectroscopic ellipsometry. The refractive index of ZONE exposed at 100 mJ/cm^2 is still around 1.55 at 632 nm, which is far from the ZnO refractive index.[38] A B-spline model was built to understand the optical property in the absorptive region, as shown in Fig.S2. The oscillation around 3.3 eV only increases insignificantly and no bandgap was observed, contrary to its behavior upon thermal treatment. This implies that although upon EUV exposure some organic bonds are cleaved and the photoresist switches its solubility, no pure zinc oxide is formed. Hence, compared to thermal decomposition where all ligands seem to be cleaved at the same rate, only partial ligand cleavage is induced by EUV radiation and is sufficient to switch the solubility.

The exposed ZONE was then measured furthermore by XPS to understand the elemental change during EUV exposure. In Fig.10 (a), when the signal was normalized to the Zn intensity as explained above, we found that during EUV exposure (100 mJ/cm^2) only around 40% of nitrogen was lost, which fits with the observation in outgassing (Fig. 9(b)), compared to the previously discussed obvious loss of carbon and nitrogen when baked at 140 °C or higher for 1 minute. For the carbon and oxygen signals, however, we noticed a slight increase after EUV exposure. This is probably due to the contamination by carbon during storage in atmospheric conditions and the uptake of moisture. Yet, XPS is a very surface sensitive technique that is limited to the surface, while FTIR probes the average bonding state over the whole film volume. During thermal bake the overall strong loss of the organic atoms surpass the absorbed surface contamination. Therefore, we only observed the clear net reduction of the signals. During EUV exposure, there is an insignificant change in the carbon and oxygen signals. Therefore, the absorption of carbon and moisture became more obvious. We also noticed that at this EUV dose the ZONE resist was condensed and a development of 15

seconds by DP819A led to no thickness loss. By contrast, ZONE resist with a bake of 140 °C without EUV exposure can be developed under the same condition. The difference in solubility suggests that during baking at 140 °C compared to EUV exposure (100 mJ/cm^2), the underlying reactions are distinct: the former involves indiscriminate bond cleavage, while the latter proceeds through preferential bond cleavages. To further understand the binding state of oxygen after EUV exposure, a fitting of the O1s peaks was performed using CasaXPS and is shown in Fig. 10 (b). The oxygen related to the carboxylate oxygen (peak 2) is observed to change insignificantly during EUV exposure compared to a bake of 180 °C, yet no signal is identified as Zn-O bond (peak 3). The O1s spectra could be fitted very well with employing only two peaks (See Fig.S9). Instead, the peak 1 around 531.6 eV which is related to organic and metal hydroxide species, the hydroxyl species increased slightly.[17] This may be explained by moisture uptake by the exposed ZONE, which is linked to the observation of the appearance of a broad -OH band in EUV exposed films that were exposed to clean room air, but is absent when the film is transferred in vacuum from the exposure tool to the FTIR spectrometer.

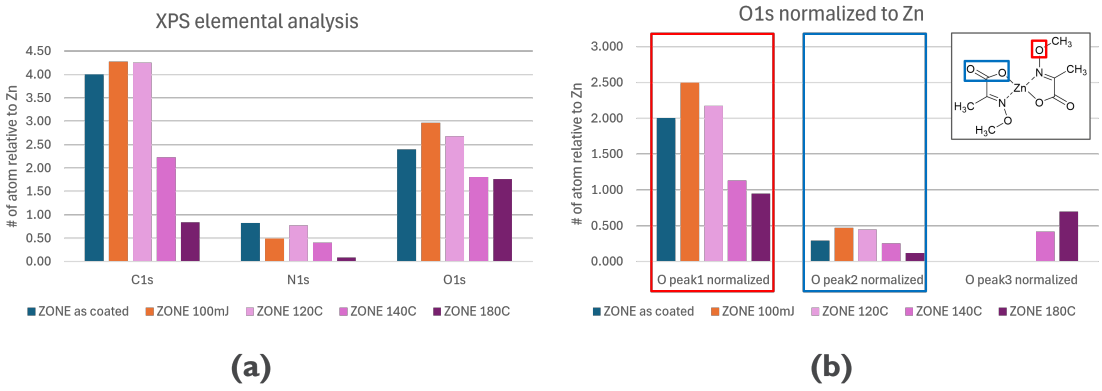

Figure 10: (a) XPS elemental analysis for samples after EUV exposure (100 mJ/cm^2) and bake normalized to the Zn signal. (b) Deconvoluted O1s signal.

In conclusion, upon EUV exposure, the C–C bond (marked red in Fig. 9 (a)) connecting the methyl-substituted oxime group to the carbonyl backbone is likely more susceptible to cleavage. Thermal decomposition, as discussed in the previous section, of the ZONE

resist is associated with indiscriminate cleavage of organic bonds. As a result, the reaction mechanism during baking is dominated by overall decomposition, converting the film into zinc oxide even within a relatively short timescale of minutes. In contrast, no evidence of zinc oxide formation during EUV exposure was observed based on spectroscopic ellipsometry and XPS analysis. The slight increase of the O 1s peak at 531.6 eV suggests a capture of air moisture of the exposed ZONE. From FTIR we also noticed that there was a higher depletion for the CCO bending mode compared to the depletion of the C=O vibration. This could imply that the depletion of CCO and C=O were contributed by the cleavage of C-C (adjacent to the carbonyl backbone). However, in practice, it is difficult to perform a detailed quantitative assessment of FTIR spectra, as these signals are convoluted and overlapping. Subtle structural changes in other parts of the molecule may also influence the vibrational features of the functional groups under investigation. Further FTIR analysis also revealed that different organic bonds are cleaved at different rates upon EUV exposure. A significantly higher cleavage rate was observed for N–O bonds, while cleavage of C–H and CH_3 groups was comparatively lower (Fig. 9(a)). Additionally, the formation of N–H stretching modes was detected (Fig. 8), which is consistent with the cleavage of N–O bonds. However, the newly formed N–H bonds cannot bridge between ZONE molecules. We didn't observe any new organic bond formation except for N–H bonds. These results suggest that the film is more likely to undergo a solubility switch due to N–O bond cleavage and N–H formation, rather than through network formation. This conclusion is supported by the absence of Zn–O bonds in the XPS analysis and the lack of new organic bond signals (other than N–H) in FTIR measurements. Notably, ZONE films exposed to 100 mJ/cm^2 EUV could still be dissolved by a 60-second water rinse. This indicates that no new covalent bonding occurred between zinc oximate molecules—neither through organic crosslinking, nor Zn–O network formation, as confirmed by the O 1s XPS data. If such a crosslinked network had formed, either via organic or inorganic bonds, the film would be insoluble in both developer and water. Therefore, we hypothesize that the solubility switch in the ZONE resist arises

from partial ligand cleavage. At higher EUV doses, more molecules experience preferential ligand loss, resulting in reduced local solubility in the developer. Finally, the surface energy of the exposed ZONE resist was determined by contact angle measurements. Before EUV exposure, the dispersive component was 23.03 mJ/m^2 and the polar component was 40.02 mJ/m^2. After EUV exposure, the dispersive and polar components are 25.28 mJ/m^2 and 20.43 mJ/m^2, respectively, which is not as close to the sputtered ZnO with 10% of O_2 in Najih et al. (2019)[40] as the sample baked at 180 °C. (See Fig. S11) This also supports that the film underwent a solubility change.

Conclusion

In this study, we demonstrated the promising high-resolution of pitch-24-nm line/space patterning performance of the ZONE resist, a zinc oximate-based material, although at a high dose (>140 mJ/cm^2). We provided mechanistic insights into why post-exposure bake (PEB) is not a viable process knob to reduce the EUV dose needed to achieve the desired pattern CD. Through a combination of XPS, FTIR, outgassing, spectroscopic ellipsometry, and surface energy analysis, we concluded that the ZONE resist starts thermal decomposition into ZnO from 140 °C, with just one minute of heating.

This ZnO conversion is supported by several findings: (1) complete depletion of all ligand-related vibrational features in FTIR above 180 °C, indicating indiscriminate ligand loss; (2) XPS showing significant carbon and nitrogen loss, along with the emergence of a 530 eV O 1s peak assigned to a Zn–O bond; (3) observation of organic fragments corresponding to all parts of the ligand during thermal outgassing experiment; (4) ellipsometry data showing a refractive index shift from 1.53 to above 1.7 and the emergence of a 3.3 eV optical bandgap, consistent with ZnO; and (5) surface energy measurements converging toward values reported for ZnO surfaces.

In contrast, EUV exposure induces a fundamentally different chemical mechanism. In-

stead of bulk ZnO formation, solubility switching arises from preferential ligand cleavage. Evidence includes: (1) FTIR spectra showing a milder depletion of ligands even at doses as high as 150 mJ/cm^2, with different cleaving rate of the ligands indicating a selective bond cleavage. The appearance of N–H bonds and the releasing of formaldehyde suggests N– O bond scission, which initiates the solubility switch ; (2) XPS revealing only moderate nitrogen loss (∼40%) and no significant Zn–O peak at 530 eV; (3) ellipsometry showing minimal refractive index change (1.53 to 1.55) and no observable bandgap; and (4) higher polar surface energy, inconsistent with ZnO formation.

These findings confirm that EUV exposure leads to the establishment of solubility contrast by partial ligand cleavage, while PEB promotes broad, non-selective decomposition that compromises such contrast, thus undermines the pattern fidelity. In the EUV exposed region during PEB, the molecules with partial ligand lost that led to the solubility switch could lose other ligands, therefore the built-up solubility contrast diminished. As a result, we observed increased LER at 120 °C and resolution loss at 140 °C. ZONE performs well even at the pitch-24-nm L/S pattern, which is the highest resolution of 0.33 NA EUV scanner, but its sensitivity cannot be enhanced through thermal processing—unlike many conventional chemically amplified resists. To fully leverage the promise of metal oximate systems in EUV lithography, future work is needed to explore tuning of the metal center or ligand structure to mitigate thermal decomposition and enable better PEB compatibility.

Acknowledgement

The authors would like to thank Materials & Components Analysis (MCA) group, Ilse Hoflijk and Inge Vaesen, at imec for their help with XPS analysis. The authors would also like to thank imec colleagues Jelle Vandereyken, Nadia Vandenbroeck, Philippe Foubert, and Shreya Basak for their support with the lithography and track process. This work has been enabled in part by the NanoIC pilot line. The acquisition and operation are jointly funded

by the Chips Joint Undertaking, through the European Union's Digital Europe (101183266) and Horizon Europe programs (101183277), as well as by the participating states Belgium (Flanders), France, Germany, Finland, Ireland and Romania. For more information, visit nanoic-project.eu. The authors declare no conflict of interest. B.H. (senior research associate) acknowledges funding from the F.R.S.-FNRS and financial support from the ARC project DREAMS (21/26.116).

Supporting Information Available

S1. CD-SEM images: Degrade from nano-resolution to micro-resolution with PEB at 140°C

This is further investigation of Fig. 3(c) that we learned no line-and-space nano-sctructure form after EUV exposure. In this image, we further zoom-out with a very large field of view of 22.5 µm X 22.5 µm. We found that not all the photoresist was washed away during development, instead structure of sub-micro-meter resolution still printed. Therefore, the ZONE resist in the patterned region may experience lost of local solubility contrast.

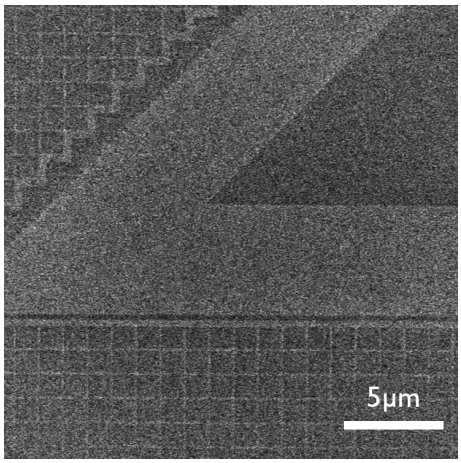

Figure S1: From the patterning wafer at PEB=140°C, alignment mark was observed with FOV of 22.5 µm X 22.5 µm. This implied that the ZONE resist is still capable of printing but lost resolution due to the lost of solubility contrast.

S2. Tauc plot for EUV exposed ZONE resist

To further investigate the EUV exposed effect compared to bake effect with ellipsometry (Fig. 5), we built a b-spline model as we did in Fig. 5. We noticed that after EUV exposure at 100 mJ/cm^2, we only see slightly increase of oscillation around 3.4 eV and a plateau between 3 to 3.3 eV. No obvious band gap formation observed. This indicates the dose that we use for EUV patterning (100 mJ/cm^2) does not induce the formation of zinc oxide.

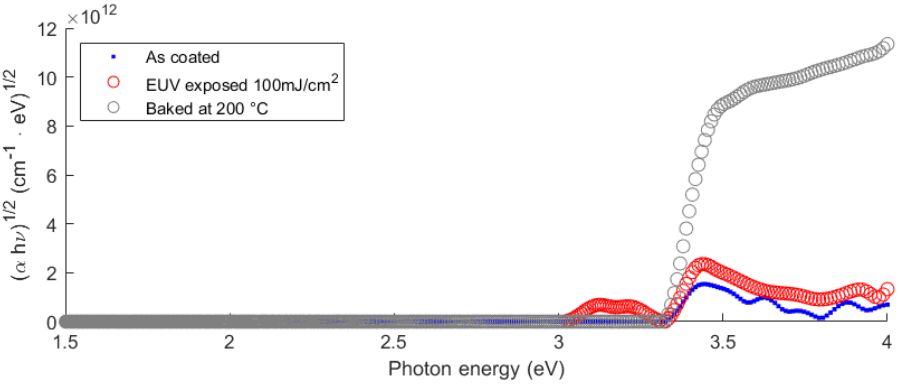

Figure S2: Tauc plot for ZONE before and after 100 mJ/cm^2 EUV exposure, built by b-spline model with the extracted thickness with Cauchy model from transparent region (400 nm to 1000 nm). The oscillation only increased slightly and a new mild oscillation appeared at around 3.3 eV. No bandgap was observed as in Fig. 5.

S3. Kinetic fitting of pure thermal reaction

To determine whether all ligands exhibit similar behavior during thermal baking, we applied a simple first-order rate constant model, denoted as k_T, as described by the Arrhenius equation. In this equation, E_a represents the activation energy, a1 is the Arrhenius pre-exponential factor, R is the ideal gas constant, and T is the bake temperature. We used the ligand signal from Fig. 4(b) for kinetic fitting. The results confirm that all ligands are cleaved with the same kinetic constants, providing quantitative evidence that they decompose at the same rate, which was also visually apparent in Fig. 4(b).

$$ligand\ signal \propto e^{-k_T t}, k_T = \alpha_1 e^{-\frac{E_a}{RT}}$$

	C=N C=O	C-N-O	CH	CH3	d-CCO	OCO	v-CCO
Ea	6.58E+04	6.60E+04	6.70E+04	6.59E+04	6.66E+04	6.65E+04	6.62E+04
a1	3.17E+06	2.87E+06	3.54E+06	2.87E+06	3.54E+06	3.11E+06	3.26E+06

Figure S3: Kinetic fitting of ligand signal when bake at different temperature. The activation energy Ea is around the same value for different ligands, and all ligands' a1 are around the same order.

S4. Kinetic fitting value of C upon EUV exposure

We visualized the C value in Fig. 9 (a), here is the exact fitting values with the error bar. The differences of C value are greater than the error bars. Therefore, indicates the different bond cleavage rate upon EUV exposure. The raw data of the integrated ligand signal is shown in Fig. S5, where each signal is normalized to the unexposed ligand signal. As the EUV dose increases, the difference of ligand cleavage rate for different ligands also increases.

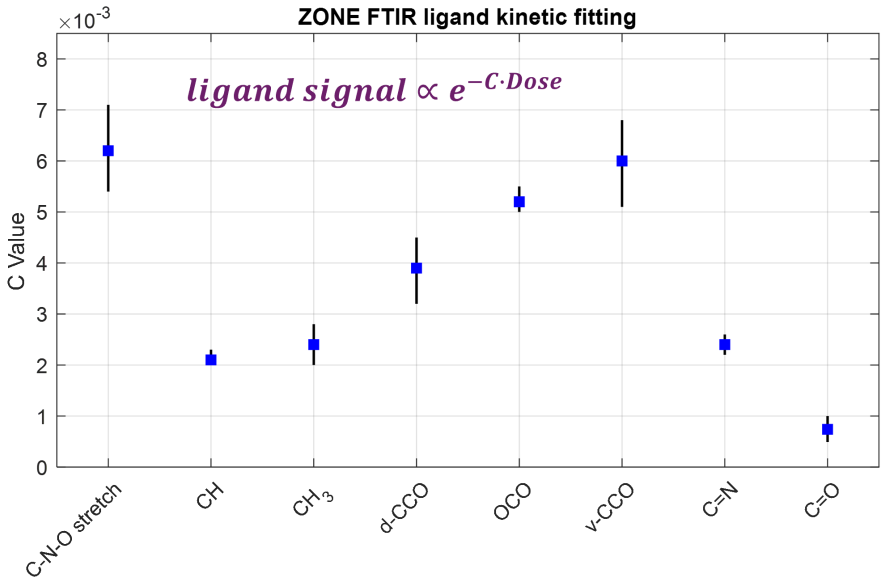

Figure S4: Kinetic fitting of the ligand signal as a function of EUV exposure dose. A significant change in the fitted parameter C was observed, with non-overlapping error bars indicating high confidence in the preferential bond cleavage induced by EUV exposure.

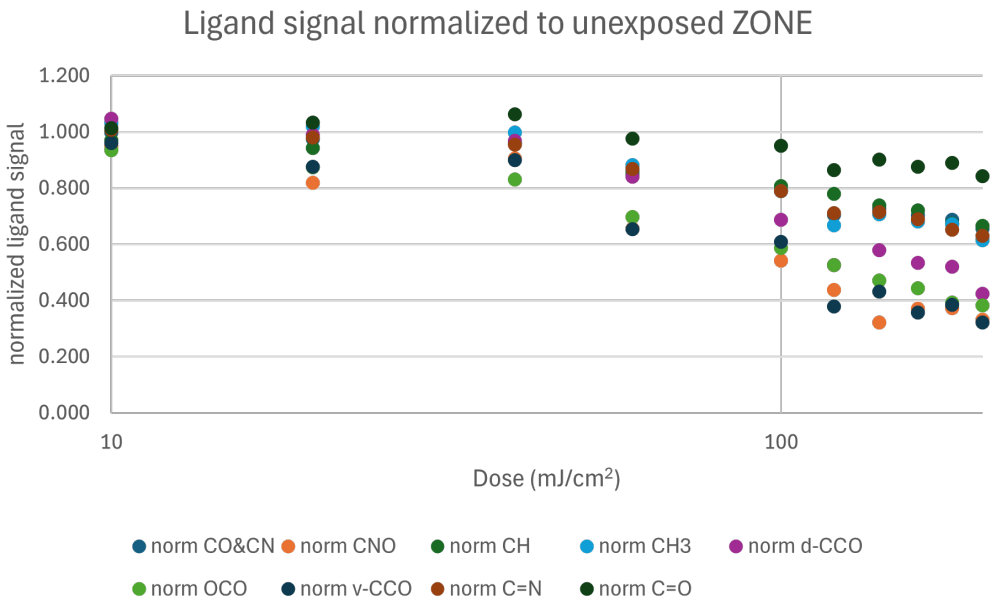

Figure S5: Raw data of all the ligands signal before kinetic fitting. The ligand signals are normalized to the unexposed film.

S5. Thickness loss during exposure at different EUV dose

To understand when the ZONE resist is fully condensed, we made a contrast curve exposure and measured the thickness before and after exposure. No thickness loss when dose is higher than 40 mJ/cm^2 during a development with DP819A for 15 seconds.

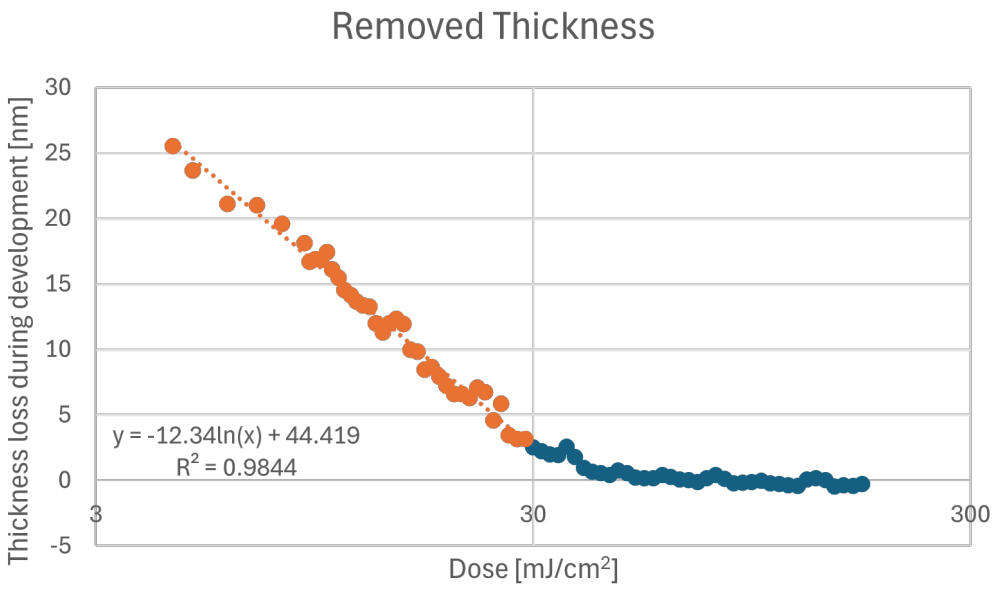

Figure S6: Thickness loss of a contrast curve wafer exposed in NXE3400:B after development with DP819A for 15 seconds. There was no significant thickness loss when the exposure dose was higher than 40 mJ/cm^2. Orange datapoints were used for the linear fit.

S6. ZONE RGA data v.s. Normalized NIST spectra

We used the NIST data base for 4 different species: CH_2O, CH_3OH, CH_3CN, and CO_2, to synthesize a RGA spectra by normalize the highest peak of our measured spectra. We added the normalized 4 signals together, as the lower plot of Fig. S7 shows. This NIST database synthesized fit (orange) matches well with our ZONE RGA data (blue) in the upper part of Fig. S7.

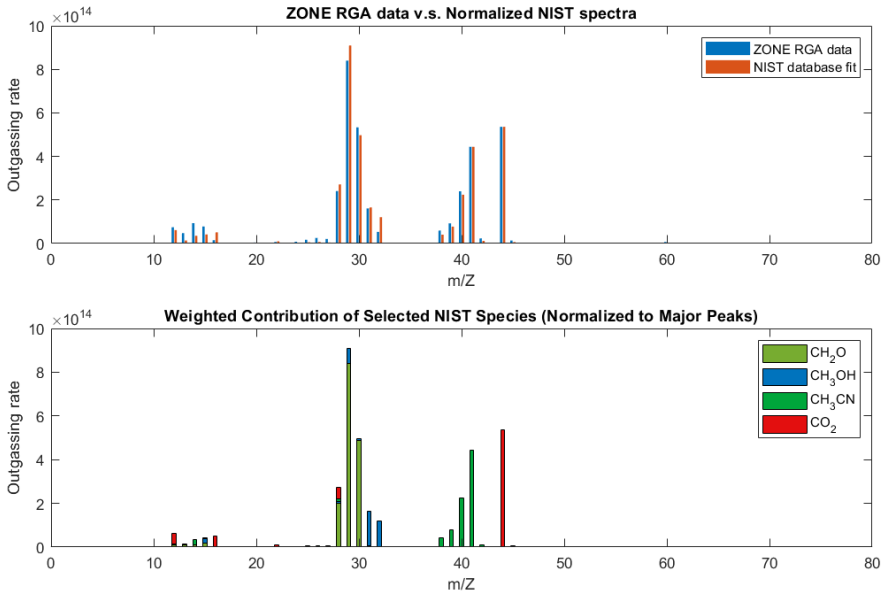

Figure S7: RGA mass spectra of ZONE fitted using identified species from the NIST database. The upper figure shows the raw data along with the summed fit. The lower figure presents a stacked bar chart of the individual species contributions.

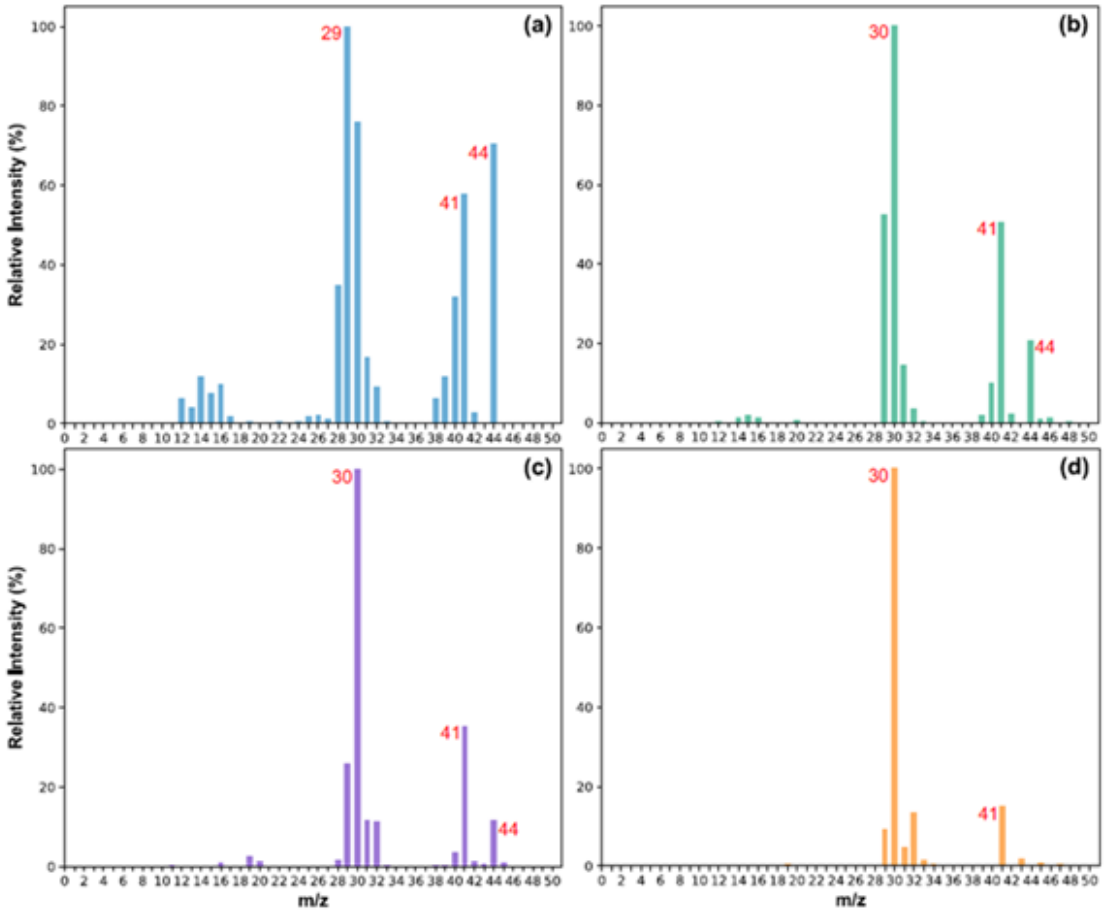

Figure S8: ZONE mass spectra during EUV exposure with different RGA ionization energy (a) 50 eV, (b) 20 eV, (c) 17 eV, and (d) 15 eV

S7. XPS raw data and the fitting

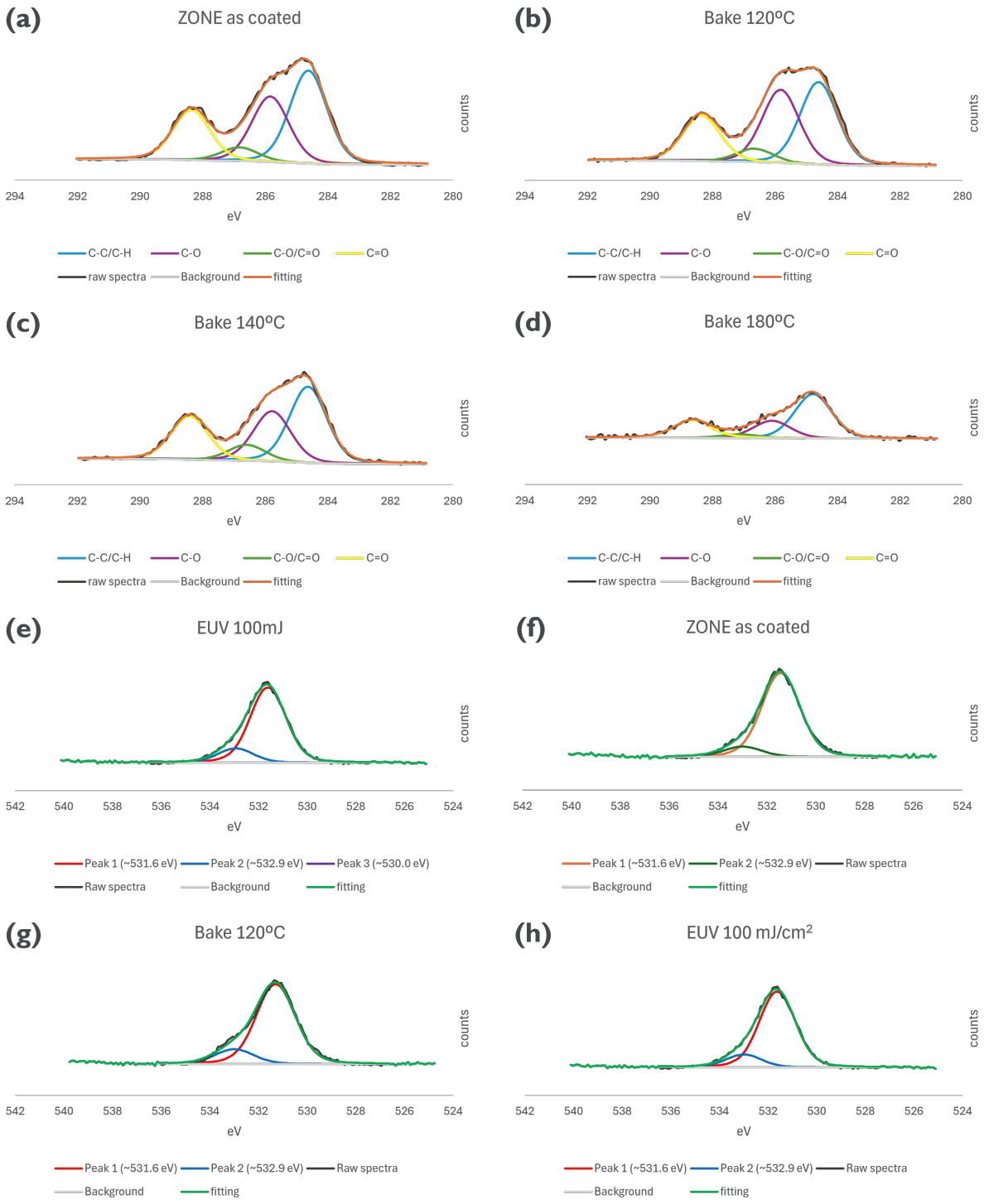

Figure S9: XPS O1s fittings of ZONE films: (a-e) Fitting with three peaks: as coated, baked at 120°C, 140°C 180°C, and (e) after EUV exposure 100mJ/cm^2. (f-h) Fitting with two peaks: as coated, baked at 120°C, and EUV exposure 100mJ/cm^2. For as coated, baked at 120°C, and EUV exposure samples, two peaks fitting show no difference to three peaks fitting. Therefore, we concluded that there is no zinc oxide components within these samples.

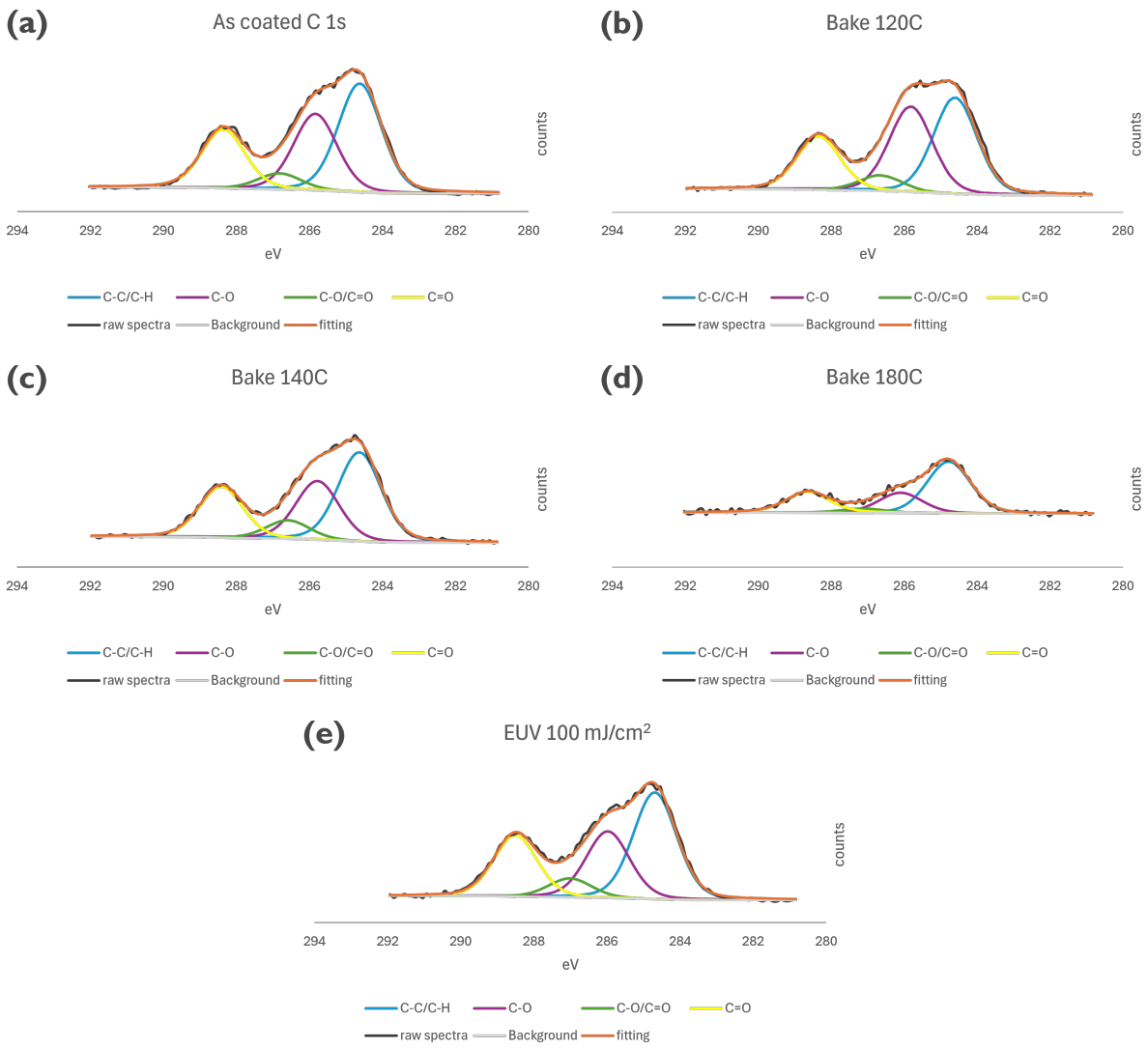

Figure S10: XPS C1s fittings of ZONE films: (a) as coated, (b–d) baked at different temperatures, and (e) after EUV exposure.

S8. Surface energy analysis from contact angle measurement

To probe the interfacial properties of the film, we measured the contact angles of water and diiodomethane. After baking at 180 °C for 1 minute, the polar component of the surface energy decreased markedly, and the overall surface energy became comparable to that of sputtered ZnO reported by Najih et al. (2019).[40] In contrast, while EUV exposure at 100 mJ/cm^2 also reduced the polar component of ZONE, its surface energy remained clearly distinct from that of ZnO described by Najih et al. (2019).

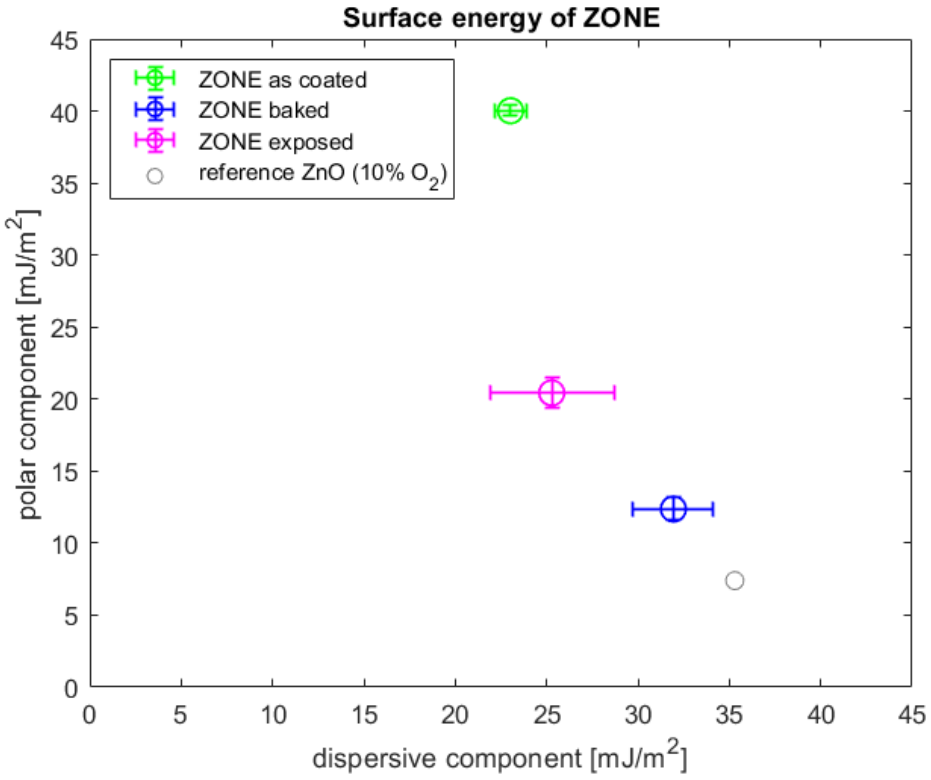

Figure S11: Surface energy of ZONE films determined by contact angle measurements using water and diiodomethane. Measurements were performed without development. The green dot represents the as-coated film, the blue dot represents the film baked at 180 °C for 1 minute, and the pink dot represents the film exposed to 100 mJ/cm^2 EUV dose. The grey dot represents the reference sputtered ZnO surface energy from Najih et al. (2019).[40]

References

(1) Moore, G. E.; others Cramming more components onto integrated circuits. 1965.

(2) Ober, C. K.; Käfer, F.; Yuan, C. Recent developments in photoresists for extreme-ultraviolet lithography. *Polymer* **2023**, *280*, 126020.

(3) De Simone, D.; Vanelderen, P.; Vandenberghe, G. Photo material readiness at the eve of EUVL HVM. *Journal of photopolymer science and technology* **2017**, *30*, 613–617.

(4) De Bisschop, P.; Hendrickx, E. Stochastic printing failures in EUV lithography. Extreme Ultraviolet (EUV) Lithography X. 2019; pp 37–56.

(5) Vesters, Y.; De Simone, D.; De Gendt, S. Influence of post exposure bake time on EUV photoresist RLS trade-off. Extreme Ultraviolet (EUV) Lithography VIII. 2017; pp 439–449.

(6) Robinson, A.; Lawson, R. *Materials and processes for next generation lithography*; Elsevier, 2016; Vol. 11.

(7) Cen, J.; Deng, Z.; Liu, S. Emerging trends in the chemistry of polymeric resists for extreme ultraviolet lithography. *Polymer Chemistry* **2024**, *15*, 4599–4614.

(8) Ito, H. Chemically amplified resists: past, present, and future. *Advances in Resist Technology and Processing XVI* **1999**, *3678*, 2–12.

(9) Li, J.; Li, H. Impact of chemical stochastics in extreme ultraviolet photoresists on the pattern quality. *AIP Advances* **2025**, *15*, 035236.

(10) Schmid, G. M.; Stewart, M. D.; Singh, V. K.; Willson, C. G. Spatial distribution of reaction products in positive tone chemically amplified resists. *Journal of Vacuum Science & Technology B: Microelectronics and Nanometer Structures Processing, Measurement, and Phenomena* **2002**, *20*, 185–190.

(11) Saifullah, M. S.; Tiwale, N.; Ganesan, R. Review of metal-containing resists in electron beam lithography: perspectives for extreme ultraviolet patterning. *Journal of Micro/Nanopatterning, Materials, and Metrology* **2022**, *21*, 041402–041402.

(12) Lim, G.; Lee, K.; Choi, S.; Yoon, H. J. Organometallic and coordinative photoresist materials for EUV lithography and related photolytic mechanisms. *Coordination Chemistry Reviews* **2023**, *493*, 215307.

(13) Grenville, A.; Anderson, J. T.; Clark, B. L.; De Schepper, P.; Edson, J.; Greer, M.; Jiang, K.; Kocsis, M.; Meyers, S. T.; Stowers, J. K.; others Integrated fab process for

metal oxide EUV photoresist. Advances in Patterning Materials and Processes XXXII. 2015; pp 225–232.

(14) Hill, M. R.; Jones, A. W.; Russell, J. J.; Roberts, N. K.; Lamb, R. N. Towards new precursors for ZnO thin films by single source CVD: the X-ray structures and precursor properties of zinc ketoacidoximates. *Inorganica chimica acta* **2005**, *358*, 201–206.

(15) Schneider, J. J.; Hoffmann, R. C.; Engstler, J.; Dilfer, S.; Klyszcz, A.; Erdem, E.; Jakes, P.; Eichel, R. A. Zinc oxide derived from single source precursor chemistry under chimie douce conditions: formation pathway, defect chemistry and possible applications in thin film printing. *Journal of Materials Chemistry* **2009**, *19*, 1449–1457.

(16) Hoffmann, R. C.; Dilfer, S.; Issanin, A.; Schneider, J. J. Solution processed ZnO–Challenges in processing and performance on flexible substrates. *physica status solidi (a)* **2010**, *207*, 1590–1595.

(17) Sanctis, S.; Hoffmann, R. C.; Bruns, M.; Schneider, J. J. Direct photopatterning of solution–processed amorphous indium zinc oxide and zinc tin oxide semiconductors—A chimie douce molecular precursor approach to thin film electronic oxides. *Advanced Materials Interfaces* **2018**, *5*, 1800324.

(18) Hoffmann, R. C.; Schneider, J. J. A Photochemically Induced Molecular Pathway to Smooth and Transparent Gallium-Doped Zinc Oxide Ceramic. *Journal of the American Ceramic Society* **2011**, *94*, 1878–1883.

(19) Saifullah, M. S.; Rajak, A. K.; Hofhuis, K. A.; Tiwale, N.; Mahfoud, Z.; Testino, A.; Karadan, P.; Vockenhuber, M.; Kazazis, D.; Valiyaveettil, S.; others Approaching Angstrom-Scale Resolution in Lithography Using Low-Molecular-Mass Resists ($<$ 500 Da). *ACS nano* **2024**, *18*, 24076–24094.

(20) Kawakami, S.; Onitsuka, T.; Kamei, Y.; Shimura, S.; Park, C. H.; Lee, S. H.; Lee, H. G.; Seo, J. W.; il Kim, J.; ho Roh, J.; others Metal oxide resist (MOR) EUV lithogra-

phy processes for DRAM application. Advances in Patterning Materials and Processes XXXIX. 2022; pp 177–182.

(21) Pollentier, I.; Rathore, A.; Gupta, M.; De Simone, D.; Suh, H. S. To bake or not to bake...: the impact of prebake in the EUV resist process. Advances in Patterning Materials and Processes XXXIX. 2022; pp 42–48.

(22) Haitjema, J.; Zhang, Y.; Vockenhuber, M.; Kazazis, D.; Ekinci, Y.; Brouwer, A. M. Extreme ultraviolet patterning of tin-oxo cages. *Journal of Micro/Nanolithography, MEMS, and MOEMS* **2017**, *16*, 033510–033510.

(23) Needham, C. D.; Welling, U.; Narasimhan, A.; De Schepper, P.; McQuade, L.; Kocsis, M.; Melvin III, L. S.; Stowers, J.; Meyers, S. T. Advanced simulations using an improved metal oxide photoresist model. Advances in Patterning Materials and Processes XLI. 2024; pp 243–260.

(24) Lorusso, G. F.; Beral, C.; Bogdanowicz, J.; De Simone, D.; Hasan, M.; Jehoul, C.; Moussa, A.; Saib, M.; Zidan, M.; Severi, J.; others Metrology of thin resist for high NA EUVL. Metrology, Inspection, and Process Control XXXVI. 2022; pp 229–240.

(25) Goldfarb, D. L.; Bruce, R. L.; Bucchignano, J. J.; Klaus, D. P.; Guillorn, M. A.; Wu, C. J. Pattern collapse mitigation strategies for EUV lithography. Extreme Ultraviolet (EUV) Lithography III. 2012; pp 40–52.

(26) Franke, J.-H.; Davydova, N.; Bekaert, J.; Wiaux, V.; Nair, V. V.; van Dijk, A.; Wang, E.; Maslow, M.; Hendrickx, E. Tomorrow's pitches on today's 0.33 NA scanner: pupil and imaging conditions to print P24 L/S and P28 contact holes. Extreme Ultraviolet Lithography 2020. 2021; pp 115–127.

(27) Ou, K.; Tango, N.; Fujimaki, N.; Fujimori, T. EUV CAR-NTD with new developer for stochastic reduction. International Conference on Extreme Ultraviolet Lithography 2024. 2024; pp 6–11.

(28) Lorusso, G. F.; Moussa, A.; Habashieh, S.; Van Den Heuvel, D.; Vangoidsenhoven, D.; Gupta, M.; Suh, H. S.; Chen, Y.-L.; De Simone, D.; Mack, C.; others E-beam metrology for high-NA: revisiting the imec protocol. Metrology, Inspection, and Process Control XXXIX. 2025; pp 135–147.

(29) Pollentier, I.; Dorney, K.; Piatti, L.; Holzmeier, F.; Suh, H. S. BEFORCE: An advanced, versatile platform for unravelling and quantifying EUV photoresist chemistry during exposure, processing, and interaction with the environment. Advances in Patterning Materials and Processes XLII. 2025; pp 505–512.

(30) Pollentier, I.; Vesters, Y.; Jiang, J.; Vanelderen, P.; De Simone, D. Unraveling the role of secondary electrons upon their interaction with photoresist during EUV exposure. International Conference on Extreme Ultraviolet Lithography 2017. 2017; pp 65–71.

(31) J.A. Woollam Co., Inc. RC2 Ellipsometer Datasheet. `https://www.optixs.cz/uploads/files/rc2-datovy-list-d782.pdf`, 2020; Accessed: 2025-08-05.

(32) DataPhysics Instruments GmbH DataPhysics Instruments – Measuring Instruments for Surface and Interfacial Analysis. `https://www.dataphysics-instruments.com/`, 2025; Accessed: 2025-06-24.

(33) DataPhysics Instruments GmbH Surface Energy of Solids. `https://www.dataphysics-instruments.com/knowledge-hub/surface-energy-of-solids/`, 2024; Accessed: 2025-06-24.

(34) Kaelble, D. Dispersion-polar surface tension properties of organic solids. *The Journal of Adhesion* **1970**, *2*, 66–81.

(35) Busshardt, M.; Conradi, O.; Kaminski, B.; Kürz, P.; Tschischgale, J.; Voit, A.; Hauf, M.; Zimmermann, J.; Loopstra, E.; Heil, T.; others Performance and characteristics of the NXE: 3400 optical system enabling sub-10nm node lithography (Conference Presen-

tation). International Conference on Extreme Ultraviolet Lithography 2017. 2017; p 104500D.

(36) Spectral Instruments CG6300 Spectrometer. https://spectral.se/products/cg6300, 2025; Accessed: 2025-06-24.

(37) Fractilia, Inc. Fractilia: MetroLER — LER and LCD Metrology. https://www.fractilia.com/, 2025; Accessed: 2025-06-24.

(38) Aguilar, O.; de Castro, S.; Godoy, M. P.; Rebello Sousa Dias, M. Optoelectronic characterization of Zn1-xCdxO thin films as an alternative to photonic crystals in organic solar cells. *Optical Materials Express* **2019**, *9*, 3638–3648.

(39) Yeh, C.-C.; Liu, H.-C.; Chuang, M.-Y.; Denzer, J.; Berling, D.; Zan, H.-W.; Soppera, O. Controllable Formation of Zinc Oxide Micro-and Nanostructures via DUV Direct Patterning. *Advanced Materials Interfaces* **2016**, *3*, 1600373.

(40) Najih, Y.; Adar, M.; Charafih, Y.; Rahmani, K.; Khouch, Z.; Bengourram, J.; Kouider, N.; Mabrouki, M. Characterization of ZnO thin films elaborated by cathodic sputtering with different oxygen percentages: investigation of surface energy. Journal of Physics: Conference Series. 2019; p 012015.

(41) Sagou, M.; Deguchi, T.; Nakamura, S. *Studies in Surface Science and Catalysis*; Elsevier, 1989; Vol. 44; pp 139–146.

TOC Graphic

Some journals require a graphical entry for the Table of Contents. This should be laid out "print ready" so that the sizing of the text is correct.
Inside the `tocentry` environment, the font used is Helvetica 8 pt, as required by *Journal of the American Chemical Society*.
The surrounding frame is 9 cm by 3.5 cm, which is the maximum permitted for *Journal of the American Chemical Society* graphical table of content entries. The box will not resize if the content is too big: instead it will overflow the edge of the box.
This box and the associated title will always be printed on a separate page at the end of the document.

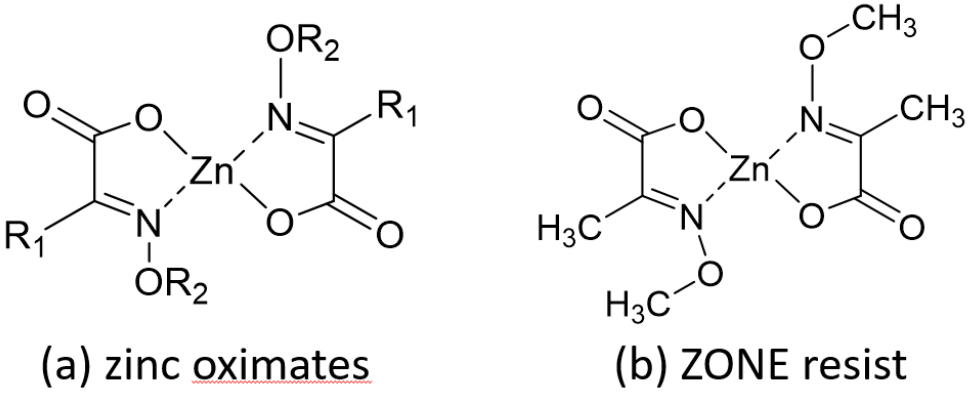

Chemical structures of (a) a generic zinc oximate with various R1 and R2 substituents, and (b) the ZONE resist with both R1 = R2 = methyl

344x144mm (72 x 72 DPI)

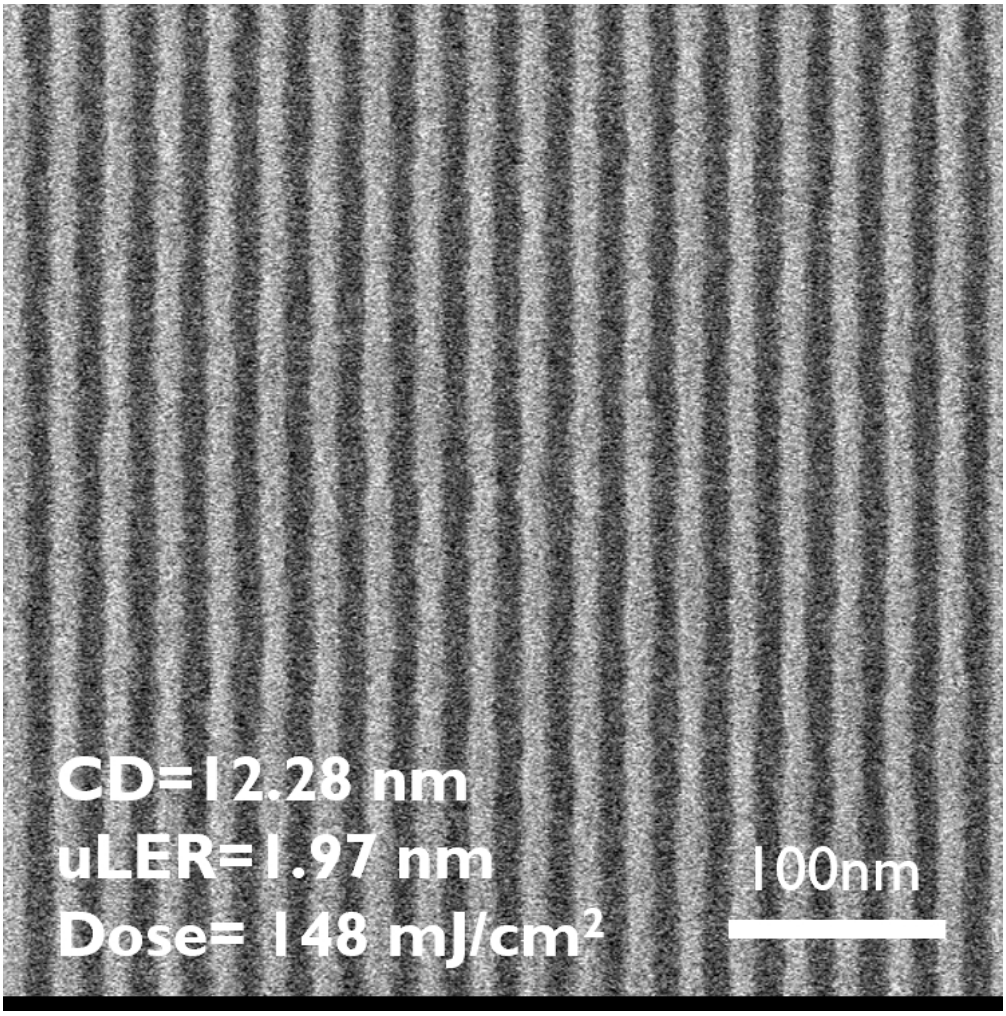

CD-SEM image of P24 L/S pattern. The development time was 15 seconds

263x264mm (72 x 72 DPI)

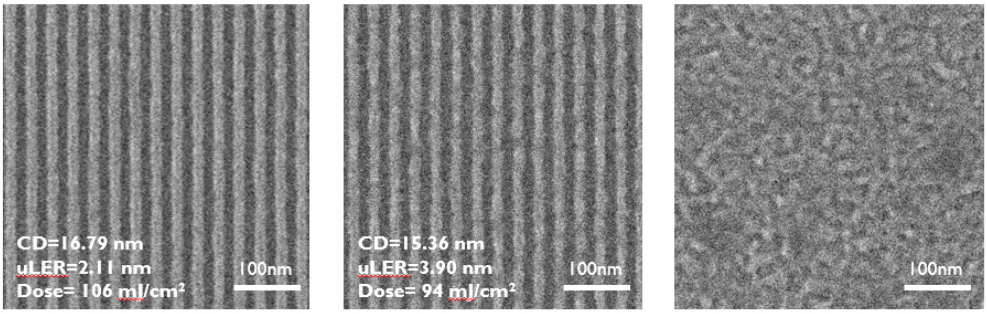

CD-SEM images of P32 L/S patterning with (a) no PEB, (b) PEB 120°C, and (c) 140 °C for 60 seconds.

490x195mm (47 x 47 DPI)

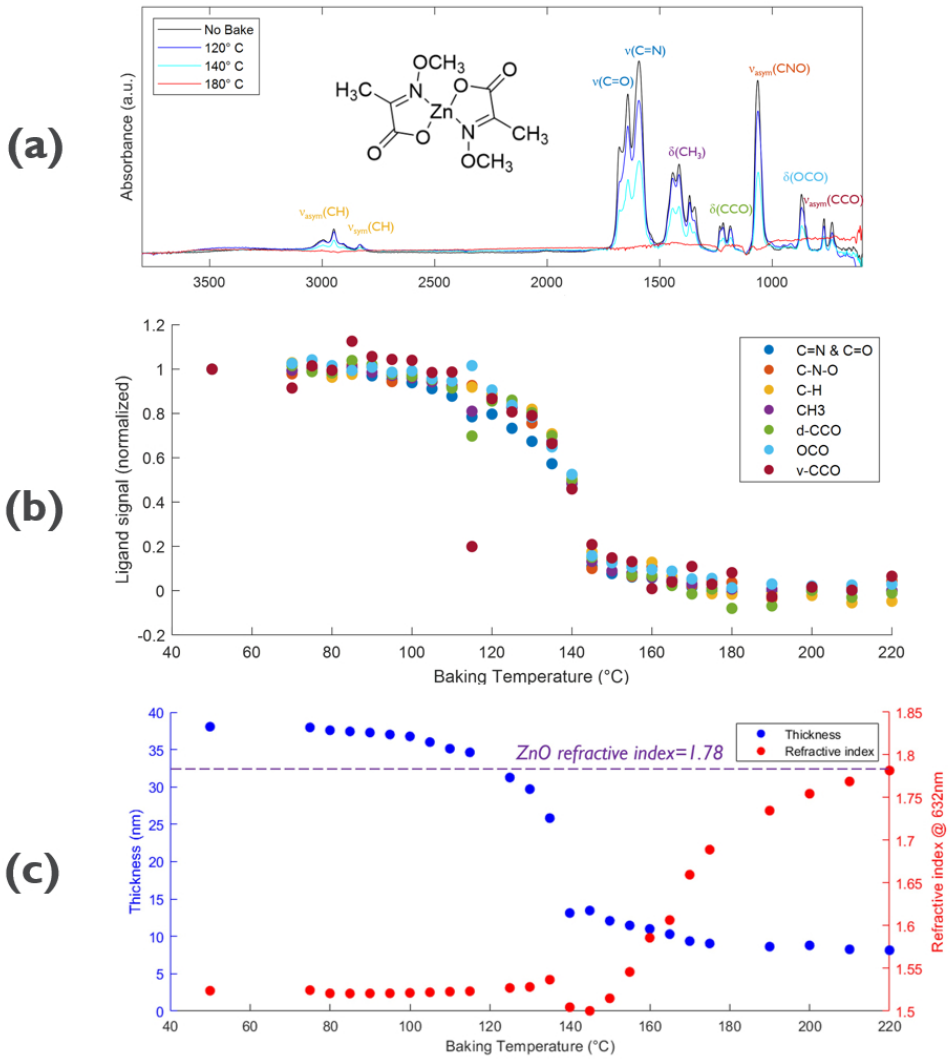

(a) FTIR spectra of unexposed ZONE with different baking temperatures: (black) No bake, (blue) 120°C, (light blue) 140°C, and (red) 180°C. The absorption peak assignments are labeled. (b) Evolution of the ligand signals as a function of baking temperature normalized to the unbaked sample. (c) Thickness and refractive index (@632 nm) as a function of baking temperature.

336x367mm (72 x 72 DPI)

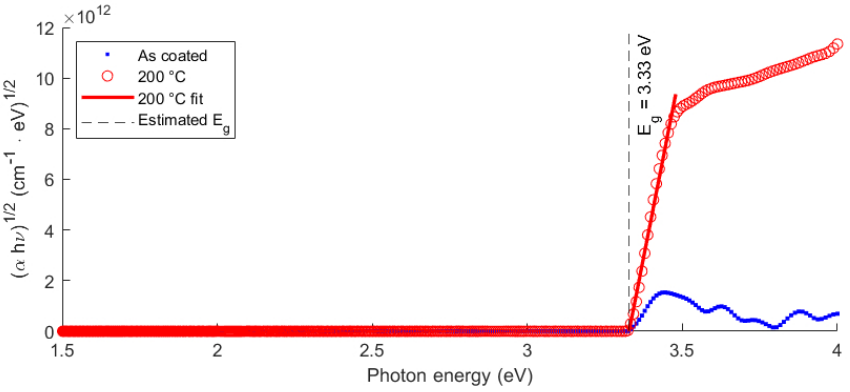

Tauc plot , i.e., the square root of the absorption coefficient multiplied by the photon energy (αhν)
1/2 as a function of photon energy (hν), for the as-coated ZONE film (blue points) and a sample baked at 200 ◦C (red points). A linear fit to the absorption edge of the baked sample (red line) allows the estimation of the optical band gap energy, Eg, by extrapolating to (αhν)
1/2 = 0, yielding Eg ≈ 3.330 eV ± 0.001eV.

335x130mm (72 x 72 DPI)

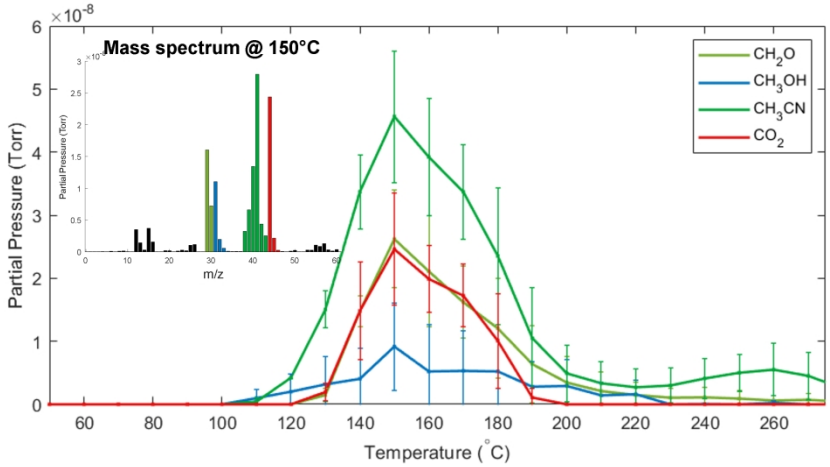

Intensity of outgassing fragments of the ZONE resist as a function of temperature.
In the inset, the complete mass spectrum at 150°C is shown with the m/z assigned to the fragments highlighted in color.

1164x550mm (72 x 72 DPI)

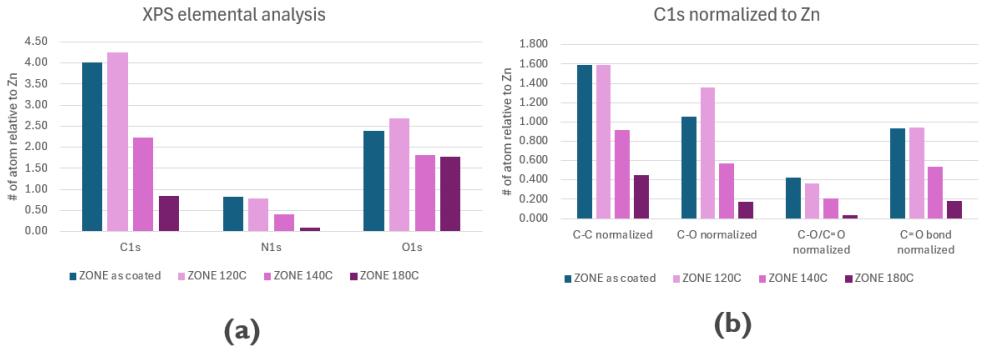

(a) XPS elemental analysis for a bake at different temperatures for 1 minute relative to Zn. When baked at 140 °C, a significant loss of carbon is observed. About 80% of carbon and 90% of nitrogen were lost after baking at 180 °C. (b) Deconvoluted C1s signal.

422x157mm (72 x 72 DPI)

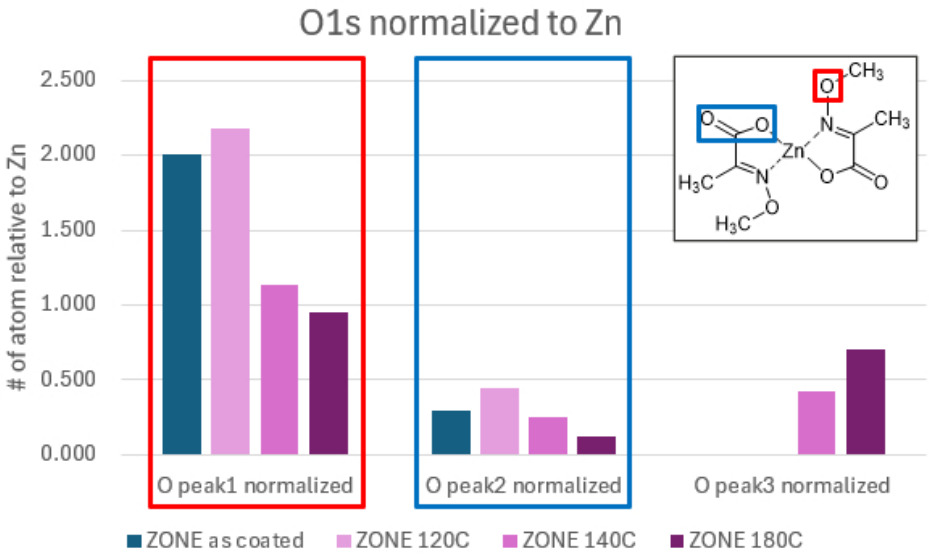

(c)

(c) Deconvoluted O1s signal. (Detail fitting of the O1s signal in Fig. S9)

218x153mm (72 x 72 DPI)

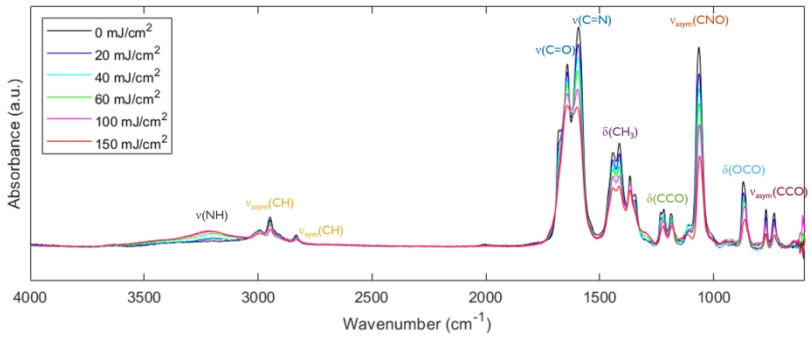

Evolution of the FTIR spectra of ZONE as a function of EUV dose. The main peaks are assigned to vibrational modes.

1164x413mm (72 x 72 DPI)

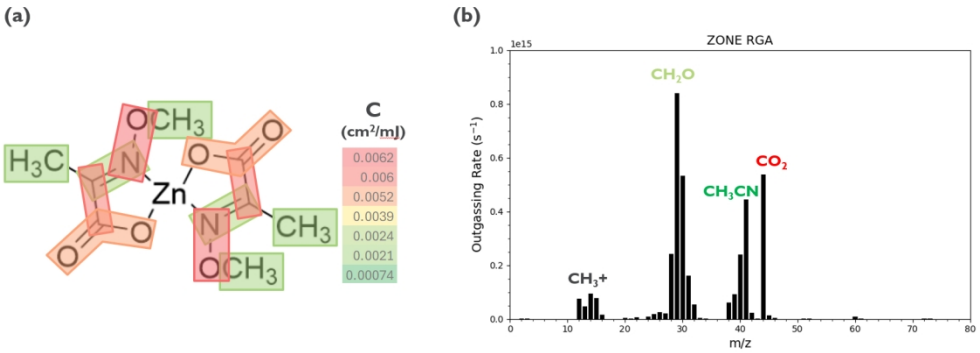

(a) Visualization of the kinetics observed in the IR spectra assigned to different parts of the molecule. The colormap represents the exponential constant C of the fit in cm2/mJ of the FTIR peak area as a function of dose. The greater the C value, the faster the bond is cleaved during EUV exposure. (Detailed C values, see Fig. S4) (b) Outgassing mass spectra for ZONE under EUV exposure. The identified species match with the interpretation of the FTIR data. For more details about the assignment, see Fig. S7

631x236mm (72 x 72 DPI)

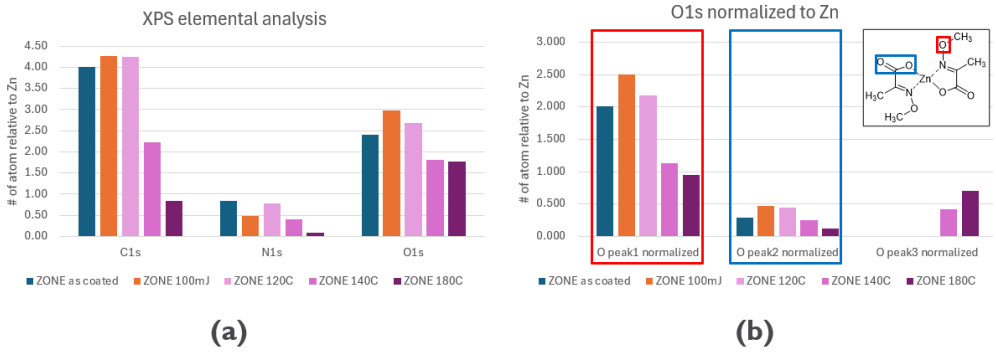

(a) XPS elemental analysis for samples after EUV exposure (100 mJ/cm2) and bake normalized to the Zn signal. (b) Deconvoluted O1s signal.

420x160mm (72 x 72 DPI)